Available online at www.sciencedirect.com
SCIENCE DIRECT
ELSEVIER
Polymer 46 (2005) 8587–8623
polymer
www.elsevier.com/locate/polymer

Feature Article

Flow-induced shish-kebab precursor structures in entangled polymer melts

Rajesh H. Somani[a], Ling Yang[a], Lei Zhu[b], Benjamin S. Hsiao[a,*]

[a]Department of Chemistry, Stony Brook University, Stony Brook, NY 11794-3400, USA
[b]Department of Chemical Engineering and Institute of Materials Science, University of Connecticut, Storrs, CT 06268, USA

Received 9 February 2005; received in revised form 31 May 2005; accepted 13 June 2005
Available online 20 July 2005

Abstract

Flow-induced crystallization has long been an important subject in polymer processing. Varying processing conditions can produce different morphologies, which lead to different properties. Recent studies indicated that the final morphology is in fact dictated by the initial formation of crystallization precursor structures (i.e. shish-kebabs) under flow. In this article, factors that affect the shish-kebab formation in entangled polymer melts are systematically reviewed, including the concept of coil–stretch transition, chain dynamics, critical orientation molecular weight, phase transition during shish and kebab formations. In particular, recent experimental results from in situ rheo-X-ray studies and ex situ microscopic examinations have been presented to illustrate several new findings of flow-induced shish-kebab structures in polymer melts. (1) The shish entity consists of stretched chains (or chain segments) that can be in the amorphous, mesomorphic or crystalline state. (2) The kebab entity mainly arises from the crystallization of coiled chains (or chain segments), which seems to follow a diffusion-control growth process. (3) A shish-kebab structure with multiple shish was seen in the ultra-high molecular weight polyethylene (UHMWPE) precursor. Based on the above results and recent simulation work from other laboratories, a modified molecular mechanism for the shish-kebab formation in entangled melt is presented.

Keywords: Flow-induced crystallization; Shish-kebabs; Polymer melts

1. Introduction

It is well-established that external flow causes orientation and extension of molecules in a polymer melt and thus affects its crystallization kinetics, structure and morphology [1–3]. Typically, the resulting bulk polymer consists of two distinct morphologies: Spherulites and flow-induced oriented morphologies (e.g. shish-kebabs) [1–21]. In this study, we are primarily concerned with the possible mechanism for the shish-kebab formation at the initial stage of flow-induced crystallization in entangled polymer melts.

Based on the conventional view, the innermost portion of the shish-kebab structure is a long and macroscopically smooth extended-chain crystalline assembly, which originates from the oriented and/or extended chains under flow. The shish provides nucleating sites (or primary nuclei) for lateral growth of folded-chain crystals or kebabs. In the 1970s, a great deal of effort was devoted to elucidate the characteristics and the molecular origin of shish-kebabs [1, 7–9]. Obviously, at the heart of the flow-induced morphology are the flow-induced changes in polymer chain conformation from the initial equilibrium random coil state. Ideally, it is desirable to be able to visually follow a single chain conformation dynamics in flow. Unfortunately, direct observation of a single molecule is difficult, especially in the case of polymer melts. Most of the early experiments, as well as theoretical developments, were concerned with the molecules in dilute solutions under elongational flow. Shear flow was often neglected as it was considered to be a 'weak' flow, due to its rotational component, unable to provide extension of polymer chains and induce shish formation [1]. Now, it is established, beyond any doubt, that even a low intensity shear field significantly affects the polymer crystallization kinetics and morphology [2].

1.1. The concept of coil–stretch transition

The first significant theoretical development was the

* Corresponding author. Tel.: +1 631 632 7793; fax: +1 631 632 6518.
E-mail address: bhsiao@notes.cc.sunysb.edu (B.S. Hsiao).

0032-3861/$ - see front matter © 2005 Elsevier Ltd. All rights reserved.
doi:10.1016/j.polymer.2005.06.034

theory by de Gennes [22], dealing with chain dynamics in dilute solutions under different types of flow. At the core of de Gennes' theory was his ingenious concept of the abrupt coil–stretch transition; i.e. polymer chains undergo a sharp transition from random coil to a fully extended-chain conformation in flow at a critical strain rate, without any intermediate stable chain conformation. The elegant studies of Keller et al. [1] provided the experimental evidence for the role of coil–stretch transition in polymer crystallization in dilute solutions under elongational flow. They demonstrated that when the strain rate was increased, there was an abrupt change in birefringence, indicative of the fully extended chain conformation, at a critical strain rate. The results led to Keller's well-known molecular model of shish-kebabs [1]. He hypothesized that the fully extended chains formed shish, and the random coils formed kebabs at a later time.

Keller reasoned that the coil–stretch transition should also exist in entangled polymer melts [1] because the actual observed flow-induced morphologies in pure melts were very similar to those observed in dilute solutions. He argued that the final morphology served as a pointer to the pre-existing state of chain extension in flow and vice versa. In other words, the shish-kebab morphology was the signature of the coil–stretch transition. The model was readily accepted by the scientific community over the last several decades, and it became a 'standard' for crystallization of entangled melts under all types of flow situations, such as elongational, shear or mixed flow.

However, to this date, direct experimental evidence for the existence of coil–stretch transition in concentrated solutions and entangled polymer melts is not available. Also, theoretical developments have not yet reached the point of a definitive prediction in these systems. This is not because of lack of effort. Many models for the polymer chain dynamics in entangled melts in flow have been developed; usually by incorporating the flow effects such as chain stretch (CS), convective constraint release (CCR), etc. in the original Doi-Edwards model [23–27]. Also, advances in the computer technology led to the development of simulation methods to predict the dynamics of chain conformations in flow [28,29]. These have been successful to a large extent in the estimation of the trends in a qualitative fashion. However, quantitative values such as the degree of chain orientation and/or extension due to the imposed flow cannot yet be determined. Experimentally, the developments of new techniques as well as the improvements in the sensitivity of old methods for the measurement of the above parameters can be seen throughout the literature [30–35]. For example, video fluorescence microscopy [30–33] and small-angle neutron scattering [34] methods have indeed allowed direct or indirect observations of the chain conformations in flow.

Results of the scientific quest have not led to a consensus among the investigators about the exact nature of the coil–stretch transition in flow—specifically, whether it is a sharp first-order transition or a continuous transition [28]. The studies of chain conformations in dilute solutions of DNA macromolecules under flow (both elongational and shear) by video fluorescence microscopy [30–33] provided strong evidence that the dynamics of the transition of a polymer chain strongly depended on the initial conformation of the chain. The history dependence suggested that not all chains could be stretched at the same time and rate. Simulation studies of Muthukumar et al. [28] indicated that, while the coil–stretch transition is discontinuous for an isolated chain in extensional flow, the dynamics of the chain extension can be deeply affected by its initial conformation. A chain can be extended by the flow and can crystallize along with other extended chains to form a shish. At the same time, another chain, identical to the previous one, can delay extension to the point that it may join other folded chains and become a part of the kebabs. Also, the presence of coiled chains has a profound effect on the coil–stretch transition. Even at very high flow rates, not all of the chains will be fully extended due to the effects of coiled chains. They concluded that polydispersity was not an essential factor for shish-kebab formation, as previously thought. This is a major diversion from the conventional view as well as previous experimental results [36–39]. In addition, Muthukumar et al. did not observe any chain where one part is partially stretched and the other part is partially folded into a crystal, as required for the conformations of microkebabs (described in later sections), which were previously thought to be formed by cilia, chains that have parts intrinsic to the shish [1]. This implies absence of microkebabs; again, a view significantly different from Keller's model of shish-kebabs.

The very existence of coil–stretch transition in entangled melts has not been well received in the rheology community. This is because polymer chains cannot undergo the coil–stretch transition without being disentangled first (de Gennes' analysis was only intended for dilute solutions), while most rheologists do not believe that chain disentanglement would occur in entangled polymer solutions or melts under typical experimental conditions. Recently, Shi-Qing Wang [40,41] published some thorough rheological and rheo-optical studies of the non-linear flow behavior of a 10 wt% polymer solution containing high molecular weight 1,4-polybutadiene (PBD, $M_w = 1.24 \times 10^6$) in oligomeric PBD ($M_w = 1$–1.5 K). They found that beyond a certain stress, comparable to the elastic plateau modulus of the entangled polymer solution, a sharp yield-like transition was observed (i.e. shear stress versus shear rate exhibited a discontinuous relationship or several orders of magnitude increase in the shear rate). These authors suggested that the molecular origin of the observed transition is due to an entanglement–disentanglement (EDT) transition. They further conjectured the following scenario for melt structure dynamics in flow. At EDT, the chains entanglements/constraints are removed and polymer chains become free as in dilute solutions. Subsequently, the free chains can undergo the coil–stretch transition due to the prevalent

stress. While the above scenario is plausible, these studies are still not an unequivocal evidence of either EDT or coil–stretch transition in the entangled state. For example, a lightly cross-linked polymer system, where chains cannot disentangle, is expected to exhibit the same rheological behavior, i.e. discontinuous relationship between shear stress and rate, as above.

The above discussion warrants a fresh look at the concept of coil–stretch transition, and the molecular origin of the shish-kebab formation in an entangled polymer melt.

1.2. Recent findings of flow-induced crystallization precursor structures

Over the past several years, our research group as well as several other groups have extensively studied the nature of shear-induced oriented structures as they evolve in polymer melts by in situ rheo-X-ray [42–60] and rheo-optical [36, 61–70] techniques and the microstructure in the bulk of fully crystallized polymer by ex situ electron microscopy methods [71–75]. It should be emphasized here that these experiments were performed only in the entangled polymer melts, under the situation of shear flow. There is no doubt that the shish-kebab morphology develops in sheared entangled melts and it is very similar to that observed in dilute or concentrated solutions under elongational or mixed flow conditions. This was not at all surprising. However, the following two observations made in recent studies of shish-kebab formation at the early stages of shear-induced crystallization were unexpected, forming the basis of this article that was intended to outline the current state of understanding and the future challenges in this subject.

(1) Combined in situ small-angle X-ray scattering (SAXS) and wide-angle X-ray diffraction (WAXD) results clearly showed that, at the early stages of crystallization in sheared polymer melts, such as polypropylene (PP), polyethylene (PE) and their blends, a scaffold (network) of precursor structures was formed [48–57]. This scaffold contained shish with extended-chain conformation that can be in either amorphous [52], mesomorphic [53,76,77] or crystalline [1–21,30] states, and kebabs with folded-chain conformation that is only in the crystalline state. It appears that the main driving force for the early stage of shish-kebab formation is dominated by primary nucleation (or homogeneous nucleation, as the phase transition is initiated from a single phase) of stretched high molecular weight chains. The formed shish-kebab scaffold ultimately dictates the subsequent polymer crystallization process, which is dominated by the unstretched random coil chains of both high and low molecular weights.
(2) The high resolution scanning electron micrographs (TEM) and SAXS patterns of sheared samples revealed that the polymer chains in the shish are neither fully stretched nor isolated [78], as previously thought. Results indicated that the chains were entangled with the neighboring chains. Although, the existence of coil–stretch transition in the melt was evidenced by the well-aligned straight shish structure, the region between kebabs did not necessarily contain one single shish, but multiple short length shish (as described in detail later) that were clearly separated from each other. The micrographs indicated that the coil–stretch transition occurred only in the sections of chains between the kebabs. Hence, we proposed, in accordance with the view of most rheologists, that individual chains do not disentangle completely in the deformed but still entangled melt and undergo abrupt unwinding to fully extended-chain conformation. The shish is indeed long; some were even >10 μm because the linear connectivity between the short, multiple shish is maintained through the entanglement points, which can be incorporated as defects in the shish assembly. The coil–stretch transition probably takes place only between the entanglement points.

At this point, it is instructive to define the precursor structure. The new school [79–84] suggests that even at quiescent conditions, the polymer crystallization is preceded by an ordered precursor (e.g. mesophase) as against a crystalline nucleus. Generally speaking, mesomorphic ordering of flexible polymer chains is based on rigidity induced by conformational ordering. For example, de Gennes and Pincus [85,86] argued that the coupling between a coil–helix transition and orientational ordering could induce a nematic phase. In polymer melts, chain mobility due to Brownian motions diminishes the probability of forming spontaneously ordered segments to a negligibly small value. However, the situation changes dramatically upon the application of a flow field, which promotes the alignment of chain segments. The chain conformation, which is assumed to be spherically symmetric before flow with an aspect ratio of ~ 1, changes significantly and the resulting aspect ratio can be very high (e.g. 10,000 in a fully extended state). This tremendous change in the aspect ratio provides considerable opportunities to form mesomorphic precursor structure for crystal nucleation.

1.3. Organization of this article

In the following, the relevant results of rheo-X-ray, rheo-optical and electron microscopy studies, old and new, are compiled to present a more concise view of the precursor structure and the molecular origin of shish-kebabs induced by flow in polymer melts. The presentation is organized as follows: In Section 2, historic background of the original shish-kebab model is briefly given; mainly for the benefit of novice readers. The high temperature (i.e. above and near the nominal melting temperature) results of isotactic polypropylene (iPP) and blend of iPP/atactic PP (aPP) in shear flow are presented in Section 3.1.1 and 3.1.2;

respectively. These results manifested the precursor structure formation in sheared melt. The effects of shear flow intensity (rate and duration or strain) are discussed in Section 3.1.3. It was found that the average chain extension reached a plateau value much below the fully extended length, even at very high values of flow intensity. This is due to the tumbling action caused by the rotational component of shear flow field. In Section 3.1.4, the observations of the precursor structures in a series of model polyethylene blends, that simulate 'dilute solution' conditions, are presented. At the chosen experimental conditions, the matrix component remained amorphous and the crystallization behavior of the minor component, ultra high molecular weight polyethylene (UHMWPE), was followed in real time. The most striking nanoscale electron micrographs of the UHMWPE shish-kebab structure are presented in Section 3.3. The pictures are strong visual evidence of the multiple shish structure and the network topology of shish-kebabs induced by shear. The large-scale micrographs are evidence of the linear connectivity of the multiple shish resulting in micron long shish-kebabs. In Section 3.3, optical micrographs (macroscopic view) of fiber-like iPP shish-kebabs are presented. In Section 4, an analytical expression was derived for the 2D small-angle scattering of a model shish-kebab structure. The average diameter, thickness and periodicity of kebabs, as well as their distributions, can be quickly estimated by fitting of the scattering data. An example of comparison of model predictions and experimental data is presented in this section. In Section 5, molecular mechanism for shish-kebab formation is discussed and the future challenges are outlined.

2. Background

2.1. Single chain dynamics during deformation (dilute solutions and polymer melts)

As mentioned above, the early developments of chain dynamics is primarily concerned with the situation of an isolated chain, which could only be realized in dilute solutions under elongational flow with no rotational components. The ingenious de Gennes theory [22] predicts that the chain will exhibit an abrupt coil–stretch transition, i.e. random coil to an extended-chain conformation, at a critical strain rate ($\dot{\varepsilon}_c$) without an intermediate stable chain conformation. de Gennes argued that the hydrodynamic interactions between chain segments vary with the degree of molecular extension. When the molecule is in a random coil conformation, only the outer segments are subjected directly to the flow field. On the other hand, all segments of a stretched chain are exposed to the flow field. Therefore, hydrodynamic interactions decrease as the molecule is stretched and polymer coil unwinds abruptly, when a certain critical value of the velocity gradient is reached. Using the simple kinetics theory for polymers, de Gennes derived an S-shaped curve (Fig. 1) for the steady-state polymer extension versus the Deborah number, 'De' ($=\tau\dot{\varepsilon}$), which represents the dimensionless flow strength and is the ratio of two intrinsic time scales: the longest polymer relaxation time (τ) and the characteristic fluid stretching time ($1/\dot{\varepsilon}$). Thus, when the elongational strain rate is gradually increased, chain segments remain in random coil conformation up to a critical strain rate ($\dot{\varepsilon}_c$), corresponding to the abrupt coil–stretch transition, beyond that they stretch out almost completely.

The elegant studies of Keller et al. [1,87–99] provided the first evidence of coil–stretch transition in dilute solutions under elongational flow, where they observed a sudden upturn in birefringence at a critical strain rate. Thus, it was established that, in steady flow, a polymer molecule can only adopt either a fully stretched or random coil conformation. No intermediate conformations are possible (intermediate states are only transients to the steady state conformation). In addition, Keller's experiments indicated that, at a given temperature, the critical strain rate ($\dot{\varepsilon}_c$) is a function of molecular weight, i.e. for a monodisperse polymer system, $\dot{\varepsilon}_c$ scales with $M^{-1.5}$ [1]. The higher molecular weight or longer chains can be extended at lower strain rates, and hence weak flows, and vice versa. In other words, at a fixed strain rate, only chains longer than a critical chain length can be stretched. The coil–stretch transition thus has two-fold criticality: (1) For a given M there is a critical $\dot{\varepsilon}$, and (2) for a given $\dot{\varepsilon}$ there is a critical M. Therefore, in a polydispersed solution, at a fixed strain rate, a bimodal distribution of the chain extension will result from flow. Chains longer than the critical M (we term it M^*) will stretch fully, while the shorter chains will not stretch and remain in random coil conformation. Increasing $\dot{\varepsilon}$ does

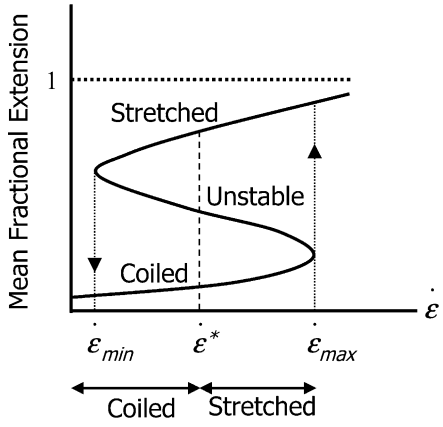

Fig. 1. Sketch of classic de Gennes coil–stretch transition curve for polymers in dilute solutions under elongational flow. Coil–stretch transition takes place at a particular value $\dot{\varepsilon}^*$ of the strain rate. Polymer molecule could exist in two physically realizable states in a narrow range of $\dot{\varepsilon}$($\dot{\varepsilon}_{min}$ to $\dot{\varepsilon}_{max}$); however, for most practical situations, hysteresis is expected, as shown by the arrows. Existence of hysteresis is a signature of sharp, first order transition. [Reprinted with permission from J Chem Phys 1974;60(12):5030. Copyright (1974) American Institute of Physics].

not affect the degree of chain extension (because of coil–stretch duality), but will increase the amount of material that becomes extended by increasingly 'cutting into' the distribution from the high molecular weight tail downwards (Fig. 2).

In concentrated solutions and polymer melts, chain overlaps and entanglements exist. The physical contacts between different chains can act as network junctions. Due to the dynamics of chain conformation, active junctions form and break up in a manner based on statistical equilibrium. The time scale of the process compared to the applied flow time scale determines the nature and degree of chain/network extension. Keller et al. [1] demonstrated that there are two critical strain rates, $\dot{\varepsilon}_c$ and $\dot{\varepsilon}_n$, in concentrated solutions under elongational flow. The first critical rate, $\dot{\varepsilon}_c$, corresponds to the coil–stretch transition; the second critical rate, $\dot{\varepsilon}_n$, corresponds to the formation of networks of stretched polymer chains. It was hypothesized that when the strain rate reaches $\dot{\varepsilon}_c$, the chains disentangle and are stretched out individually. As the strain rate increases further and reaches $\dot{\varepsilon}_n$, the chains act cooperatively like a network. At this point, the viscosity of the polymer solution increases drastically. The first critical rate was found to occur at concentrations much below the conventional overlap concentration (C^*), the inception of chain entanglements. Both critical rates decrease with the increase of concentration; but the rate of the decrease for $\dot{\varepsilon}_c$ is smaller than that for $\dot{\varepsilon}_n$ (Fig. 3(a)), which could lead to a cross-over point (Fig. 3(b)). Since the experiments for polymer melt or high concentration solutions were not performed, it was not clear whether there is a crossover at high concentrations. The existence of such a cross-over is highly important, since it implies the absence of $\dot{\varepsilon}_c$ or coil–stretch transition, i.e. a given polymer chain cannot be extended entirely, due to chain overlaps or entanglements in pure melts or high concentration solutions.

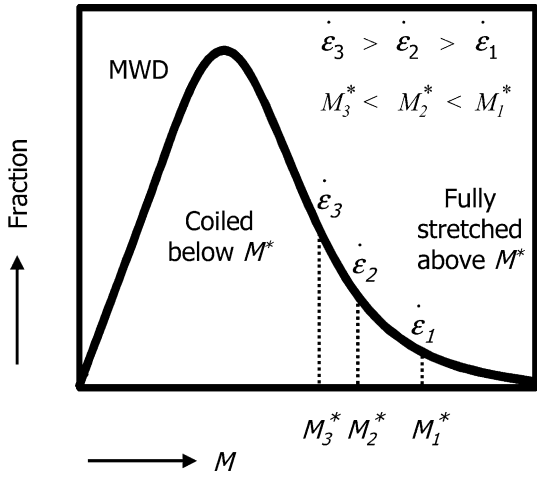

Fig. 2. Schematic plot of a molecular weight distribution showing two-fold criticality of coil–stretch transition. Increasing $\dot{\varepsilon}$ increases the amount of material by increasingly cutting into the distribution; duality of chain conformation (coiled or fully extended) is maintained. [Reprinted with permission from Processing of Polymers, edited by H.E.H. Meijer, 1997; 18:189. Copyright (1997) VCH, New York].

2.2. Shish-kebab formation in dilute polymer solutions under flow

Historically, Mitsuhashi [100] was probably the first to report the formation of fibrous 'string-like' polyethylene structures upon stirring. His work remained unnoticed for several years. Later in 1965, Pennings et al. [101] published the electron micrographs of the threads of polyethylene in stirred polyethylene solutions. These micrographs clearly showed details of flow-induced polyethylene crystalline structure. The new type of polymer crystallite consisted of two components: A central core fibril (shish) and lamellae (kebabs) strung along the core, and hence called 'shish kebabs' [1]. Shish were highly stable to the point that they can be superheated; their melting temperature was found to be 15–20 °C higher than polyethylene spherulites [101]. Therefore, it was believed that the backbone or shish of these crystallites was formed by crystallization of fully stretched/extended chains. The kebabs were believed to be folded-chain lamellar structures. The direction of growth of the kebabs was normal to the shish. The chain alignment in the kebabs was believed to be parallel to the shish.

In the early studies of shish-kebabs obtained from stirred solutions, it was noticed that the onset of the shish-kebab formation coincided with the point of occurrence of hydrodynamic instabilities and Taylor vortices [102]. It was thought that the hydrodynamics of the solution played an important role in the shish-kebab formation. However, subsequent studies provided evidence of shish-kebab formation in elongational flow without the presence of instabilities [1]. Moreover, it is now well-established that these structures occur not only in elongational but also in shear or mixed flow conditions [2]. The only requirement is that the velocity gradient parallel to the chain-axis should be sufficiently strong, above a certain critical deformation rate.

2.2.1. Current understanding of shish-kebab structure

The macroscopic view of the overall crystallization and the shish-kebab morphology in flow suggested that this texture was initiated by lines of nuclei aligned parallel to the flow direction and continued growth of lamellar crystals in a direction transverse to the flow direction (Fig. 4) [1,89]. Crystallization of extended chains is promoted for both thermodynamic and kinetic reasons. Thermodynamically, the entropy of extended chain conformation is lower than that of folded chains and thus increases the melting point of resulting crystals. Kinetically, since an extended chain is closer to its state in the crystal, it has less of a kinetic barrier to overcome than a chain in the random state. As a result, crystallization of extended chains occurs, first giving rise to shish. The shish avail themselves as nucleating templates for the coiled chains, which form folded-chain lamellae afterwards. As shown in Fig. 4, the lamellae themselves, in

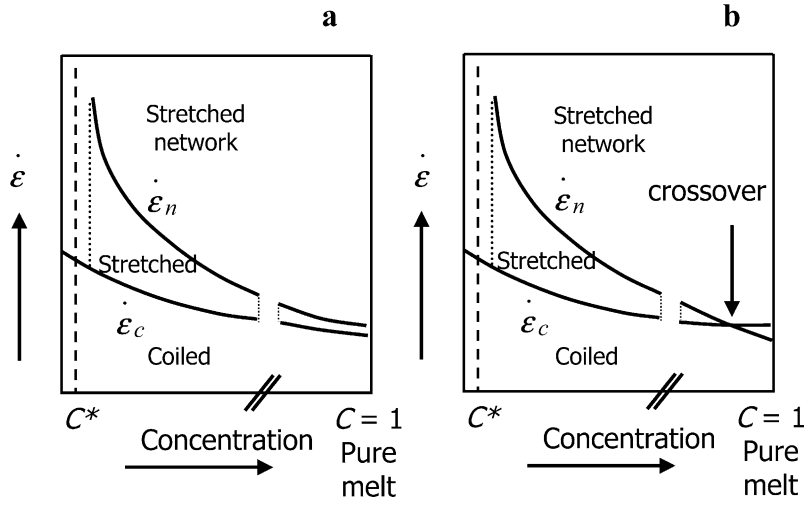

Fig. 3. Strain rate versus concentration plot showing existence of two critical strain rates in concentrated solution and melts in elongational flow; $\dot{\varepsilon}_c$ for the coil–stretch transition and $\dot{\varepsilon}_n$ for stretched network formation. Two cases are shown: (a) Finite strain window exists up to $C=1$ (pure melt) for coil–stretch transition, and (b) no strain window for coil–stretch transition at high concentrations or pure melts. [Reprinted with permission from Processing of Polymers, edited by H. E.H. Meijer, 1997;18:189. Copyright (1997) VCH, New York].

the case of PE, could twist as they do in spherulites or all be straight and parallel (lamellae chain segments parallel to the flow direction), according to whether the stress is low or high [1]. In early studies, investigations of the shish-kebab structure revealed that there are two types of kebabs [1]. One type of kebab can be flushed away by a solvent or completely melted away from the shish at high temperatures. These kebabs were referred to as 'macrokebabs'. In contrast, another type of kebab could not be flushed away even with the strongest solvent and they were found to be as thermally stable as shish. These kebabs were referred to as 'microkebabs'. The microkebabs were thought to be permanently attached to the shish core. The macrokebabs, on the other hand, were thought to have grown on the microkebab templates and not to be permanently attached to the shish.

2.2.2. Nucleation and growth of shish

Pennings et al. suggested the following mechanism for nucleation and growth of shish [101,102]. Initially, micellar nuclei develop from flow-induced extended chain segments. When a molecule sticks on the lateral surface of a micellar nucleus, it will be extended by the flow field and settle on the existing nucleus, leading to its longitudinal growth. The growth process requires winding-up of adsorbed molecules by the flow field onto the growing shish crystal. Thus, a flow field was thought to be a necessary condition for the nucleation as well as the growth of shish.

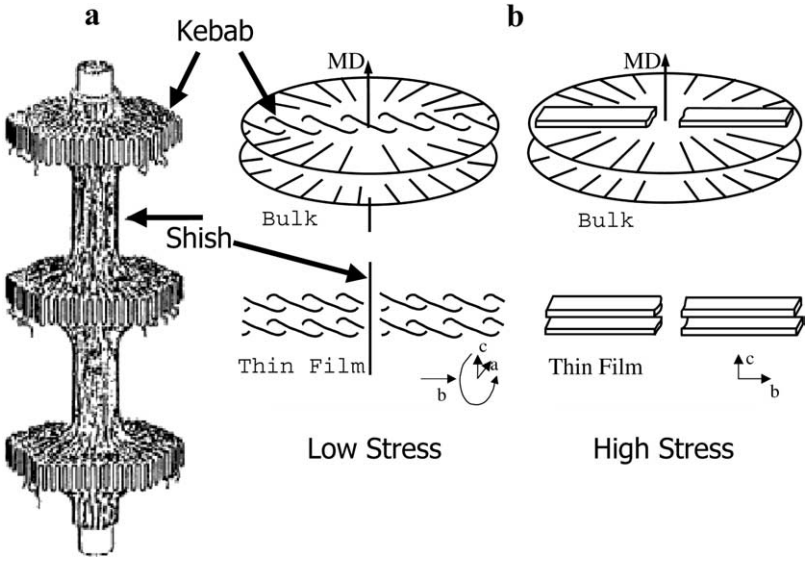

Fig. 4. Schematic model of microstructure of shish-kebab structure in polyethylene. Note the example of lamellar or kebab twisting in low stress conditions. [Reprinted with permission from Processing of Polymers, edited by H.E.H. Meijer, 1997;18:189. Copyright (1997) VCH, New York].

In 1979, Hoffman [103] explained the formation of shish crystals in quite a different way, i.e. via multiple nucleation events. In his argument, the alignment of long molecules in flow field could result in the formation of aligned micellar nuclei, which interlinked by taut tie molecules such that one macromolecule may belong to several nuclei. Subsequent crystallization would lead to the formation of long shish.

In the same year, Petermann et al. [104,105] proposed another model for the nucleation and growth of shish. Accordingly, while the external flow field is necessary for the formation of aligned micellar nuclei; its growth can be an auto-catalytic process in which the difference in free energy between the micellar nucleus and the surrounding melt induces self-orientation of the molecules in the growth front of crystallization. Further growth is continued by sucking new molecules from the relaxed melt into the growth front. As long as the growth rate of shish is large enough to over compensate the relaxation of the molecular segments on the tip of the crystals, the auto-catalytically reproduced extensional flow field can be maintained. If the growth front is too slow with respect to the segmental relaxation time, both ends of the individual molecule may be sucked into the front, forming a fold, and subsequently destroy the local orientation field. Petermann et al. concluded that the longitudinal growth of shish does not necessarily need an external flow field; a view different from that proposed by Pennings. We note that Petermann's view is consistent with the recent simulation studies of Muthukumar et al. [28], which indicated that shish growth is possible even in the absence of flow field.

2.2.3. Molecular origin of shish-kebab structure

As mentioned in Section 2.1, at the core of the early molecular theories for shish-kebab formation is de Gennes' idea of abrupt coil–stretch transition in flow with elongational component [22]. The morphology observed in the final products are the consequences of the above two extremes. The fully stretched (extended) chains form shish and the random coiled chains participate in the formation of folded-chain lamellae or kebabs. The intermediate orientations seen in partially oriented products are due to the different combinations of the two extremes, and not to intermediate chain orientations as such.

2.3. Shish-kebabs in concentrated solutions and entangled melts

In concentrated solutions and entangled polymer melts, just as in the case of dilute solutions, the dominant flow-induced crystalline structure is shish-kebabs. Often, its visibility and, hence, detectability is obscured by the surrounding crystalline material. However, the shish-kebab entities can, under certain conditions, be made conspicuously apparent by the sensitive techniques such as transmission electron microscopy (TEM) and atomic force microscopy (AFM) in real space, as well as small-angle X-ray scattering (SAXS) and wide angle X-ray diffraction (WAXD) in reciprocal space. Here, we cite the two previous, rather unique, studies that provided the images of shish at or near the transient precursor stage: (1) Schultz's TEM [106] study of shish-kebab structure development during annealing of PET fibers under stress, and (2) Petermann's [107] electron microscopic study of strained melts of polystyrene. TEM micrographs by Schultz et al. revealed that an embryonic microfibrillar structure develop at the earliest stage, the microfibril diameter was about 5 nm. Upon modest heat treatment, the microfibrils became axially punctuated with crystallites or kebabs. Furthermore, from the X-ray radial distribution function of the early stage structure, Schultz [108] estimated that in PET, the diameter of shish was about 3–4 nm in the first stage of transformation. TEM micrographs by Petermann et al. showed that the row structures of polystyrene were also thin (diameter $\sim$18 nm) and several microns long. The rod-shaped crystals exhibited a high melting temperature, about 270 °C, and Petermann conjectured that they consisted of high volume fraction of extended chain molecules.

Thus, the observed morphologies in polymer melts under flow conform closely to the elongational flow-induced structures in dilute solutions. The observations that the shish-kebab morphology in concentrated solutions and melts is similar to that in the dilute solutions led to the belief that the phenomenon of coil–stretch transition also exists under those conditions [1]. Thus, for the past four decades, the concept of coil–stretch transition was broadly applied to explain the flow-induced morphologies in polymer solutions, both dilute and concentrated, and in entangled melts under all types of flow conditions; elongational, shear and mixed.

3. New results by recent in situ and ex situ studies

Recently, several research groups have carried out in situ studies to investigate the formation of crystallization precursor structure induced by flow using newly available time-resolved characterization techniques including AFM, X-rays and birefringence. The studies of AFM, such as the works on the shish-kebab formation by Hobbs et al. [35], are particularly interesting because measurements directly revealed the structure development in real space and in real time. However, as the exact flow conditions in AFM studies are difficult to define, the technique yields mostly qualitative information.

Quantitative results during the formation of flow-induced crystallization precursor structures can be obtained by X-ray (SAXS and WAXD) and, to a lesser degree, birefringence methods. The notable rheo-optical and rheo-X-ray studies on this subject have been carried out by Winter et al. [61–64], Kornfield et al. [58–60,69,70], de Jeu et al. [76,77] and our group [48–57], just to name a few. For example, using the rheo-optical technique, Winter et al. observed that the

crystallizing melt exhibited a gel-like rheological behavior at the initial stage of flow-induced crystallization in isotactic polypropylene (iPP) [61,62]. Kornfield et al. discovered that birefringence of the deformed iPP melt exhibited an anomalous increase even at cessation of flow above the nominal melting temperature [58,70].

Using the rheo-X-ray method, de Jeu et al. reported the existence of smectic phase in deformed melt above the nominal melting temperature, where the smectic phase might form a precursor for nucleation [76,77]. Their observation was consistent with the findings of Windle et al. [109,110], who observed the existence of transient smectic mesophase in both quenched samples and during uniaxially drawing of poly(ethylene terephthalate) (PET), poly(ethylene naphthalate) (PEN) and their copolymers using synchrotron X-rays, where they concluded that the mesophase acts as a precursor of strain induced crystallization. In addition, Schultz et al. [111] studied the earliest stage of crystallization during melt spinning for four polymers: High density polyethylene (HDPE), poly(vinylidene fluoride) (PVDF), nylon 6, and poly(oxymethylene); they observed that crystallization was triggered at a critical strain level in all four polymers; probably corresponding to the highly oriented or even fully stretched but non-crystalline state of polymer chains, as in the coil–stretch transition. Recently, de Jeu et al. have composed an interesting review article [112] discussing the role of mesomorphic phase on the crystallization process in polymers (iPP, PET and poly(dimethyl siloxane) (PDMS)) containing marginal mesogenic units.

In this article, we aim to compose an overview of flow-induced crystallization precursor structures in two representative flexible polymer melts: iPP and PE, where the mesomorphic structure may or may not exist. The main body of the article will be based on our in situ rheo-X-ray studies on sheared polymer melts, and some new insight into the flow-induced shish-kebab structure will be described based on ex situ TEM measurements on solvent-extracted sheared samples. Our major goal is to discuss the nature of the first formed primary nuclei and its spatial arrangement and correlations (i.e. its landscape) under a controlled flow condition. These precursor structures essentially dictate the subsequent crystal growth and morphological development.

3.1. In situ rheo-X-ray (SAXS and WAXD) studies

To achieve the goal of characterizing the nature of the flow-induced molecular orientation and crystallization precursor structures in polymer melts, the chosen experiments should provide images (directly or indirectly, such as X-ray scattering/diffraction patterns) at the earliest stages of crystallization, typically as soon as the flow is applied. The highly sensitive synchrotron SAXS and WAXD techniques with a parallel-plate shear-stage, which was used in our studies, provided this opportunity. The in situ 2D rheo-SAXS technique gave maps of density fluctuations in the reciprocal space, which allowed us to construct a superstructure induced by flow; i.e. their orientation, spacing and relative amounts. The corresponding 2D rheo-WAXD images allowed quantitative characterization of the crystallinity, crystal orientation and crystal formation. In addition, the experiments could be performed at high melt temperatures, even above the nominal melting point of the polymer, which is of critical importance to the new findings. This is because, if the temperature is too low, the rapid crystal growth would quickly overwhelm the sought after precursor structures, as found in earlier studies [46–48]. Details of the experimental technique and procedure can be found in our previous publications. The salient features of the shear apparatus and procedure are given below.

A Linkam CSS-450 high temperature shearing stage modified for in situ X-ray scattering studies was used to precisely control shear-field and thermal history of the polymer sample. The two parallel plates of the shear stage were modified for the X-ray beam to pass through [46]. In the Linkam stage, desired shear condition is applied by rotating the bottom plate using a precision stepping motor, while the top plate remains stationary. Typically, a pressed polymer ring (outer diameter (OD) = 20 mm, inner diameter (ID) = 10 mm and thickness = 0.5–1.0 mm) was mounted between the two parallel plates of the shear stage. Prior to shear, the sample was subjected to a thermal treatment in order to ensure that the polymer melt was free of any memory effects associated with crystal aggregates and molecular orientation. The temperature protocol for shear experiments was as follows.

1. Heat the sample to a temperature above the equilibrium temperature of the polymer: 220 °C for iPP, and 165 °C for PE, at a rate of 30 °C/min.
2. Hold the temperature for several minutes (3–5 min).
3. Cool at 30 °C/min down to temperature of the experiment.
4. Maintain isothermal conditions for duration of the experiment.
5. Cool to room temperature.

SAXS and WAXD measurements were carried out at the X27C or X3A2 beamline in the National Synchrotron Light Source (NSLS), Brookhaven National Laboratory (BNL). A high resolution CCD X-ray camera was used for the recording of 2D SAXS and WAXD images. One X-ray pattern of the amorphous melt was collected immediately before shear. Subsequently, the polymer melt was subjected to the desired shear condition. 2D SAXS and WAXD patterns were collected continuously during and after cessation of shear. All X-ray data were corrected for background (air and instrument) scattering before analysis.

3.1.1. Isotactic polypropylene melt

In this section, results of several studies of an isotactic polypropylene polymer are compiled to elucidate the

present theme. The iPP sample was a Ziegler–Natta homopolymer supplied by ExxonMobil Chemical Company. Its molecular weights were: $M_n = 92{,}000$ g/mol, $M_w = 368{,}000$ g/mol and $M_z = 965{,}000$ g/mol. The nominal melting point and crystallization temperature (DSC) of this sample were 162 and 120 °C, respectively.

3.1.1.1. Step shear at 175 °C. Fig. 5 shows the rheo-SAXS and -WAXD images of the sheared iPP melt at 175 °C (i.e. 13 °C above the nominal melt point). A step-shear condition: Rate = 57 s^{-1}, strain = 1428%, was used for this experiment [49] (note that the duration of the imposed shear was only 0.25 s). The SAXS patterns clearly showed that, even at 175 °C, a large-scale oriented superstructure evolved in the polymer melt after shear. The meridional maxima parallel to the flow direction is a signature of layered structure formation having a distinctly different electron density distribution profile with respect to the surrounding melt. It is important to note that the oriented structures did not disappear even 2 h after cessation of shear, a considerably long time. On the other hand, the corresponding WAXD images did not show any crystal reflections; the pattern 2 h after shear was like the pattern of the amorphous melt before shear. Here, it should be noted that the shape of the scattering hump due to amorphous melt before and after shear is not exactly the same. In fact, it is known that the ordering of chains in the melt/precursor structures will cause small changes in its shape. For example, such behavior was clearly seen for PET fibers in the work of Schultz et al. [108], where they calculated the cylindrical distribution function by Fourier-inversion of the scattering function. Since, we are primarily interested in determining whether the early stage structures were crystalline or not, this analysis was not carried out here. However, we can conclude that the flow-induced oriented structures at this temperature must be non-crystalline or of low crystallinity below the detection limit of crystallinity in WAXD [113]. The alignment or order, both positional and orientational, of chain segments within the oriented structures is evident from their higher electron density compared to the surrounding melt and, hence, these layers may be flow-induced mesophase or precursor structures of crystal nuclei. The spacing between the layers was estimated to be about 430 Å.

The above results are direct evidence of the formation of flow-induced crystallization precursor structures in polymer melts. The flip-side of the high temperature step-shear experiment was that the concentration of shish in the precursor structure was low, or the equatorial scattering (perpendicular to the flow direction) was weak in the SAXS detection. In view of this, a slightly lower temperature of 165 °C but still above the nominal melting temperature of the iPP sample, and a more intense shear condition was used in the following set of experiments [53].

3.1.1.2. Intense shear at 165 °C. Fig. 6 shows the SAXS patterns of the sheared iPP melt at different times after a more intense shear being applied: Rate = 60 s^{-1}, duration, $t_s = 5$ s. The patterns exhibited the emergence of an equatorial streak immediately after shear (pattern at $t =$ 70 s). The equatorial streak became stronger with time, due to its further growth, evident from the SAXS images taken at subsequent time intervals ($t > 140$ s). The equatorial streaks in SAXS patterns is due to the formation of non-correlated shish parallel to the flow direction [53]. The meridional maxima emerged after the shish formation, as seen in the SAXS patterns at later times: $t = 10$, 20 and 120 min. The meridional maxima in the SAXS patterns resulted from the formation of lamellae layers (or kebabs) that are correlated and oriented perpendicular to the flow direction.

Fig. 7 shows the corresponding WAXD patterns obtained

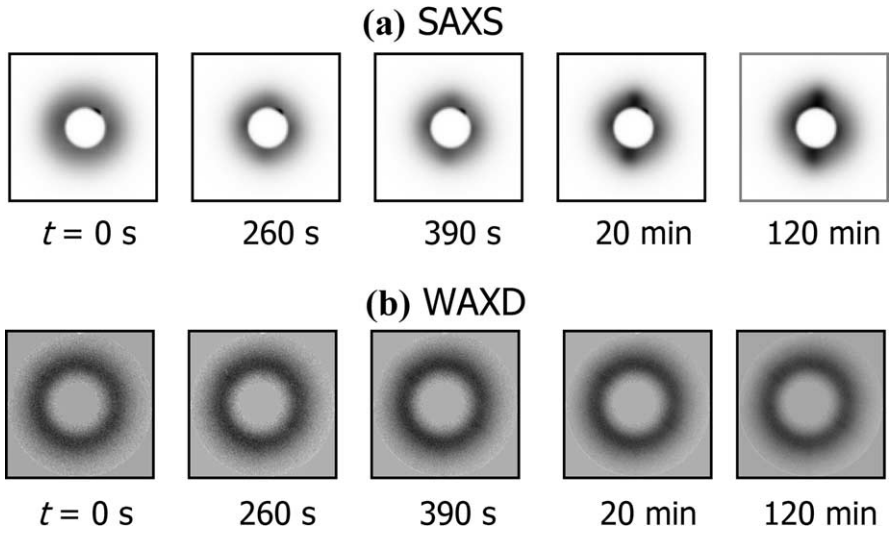

Fig. 5. (a) SAXS patterns of iPP melt at 175 °C before and after step shear (shear rate = 57 s^{-1}, strain = 1428%), (b) WAXD patterns under identical conditions of SAXS experiment. [Reprinted with permission from Physica A, 2002;304:145. Copyright (2002) Elsevier BV].

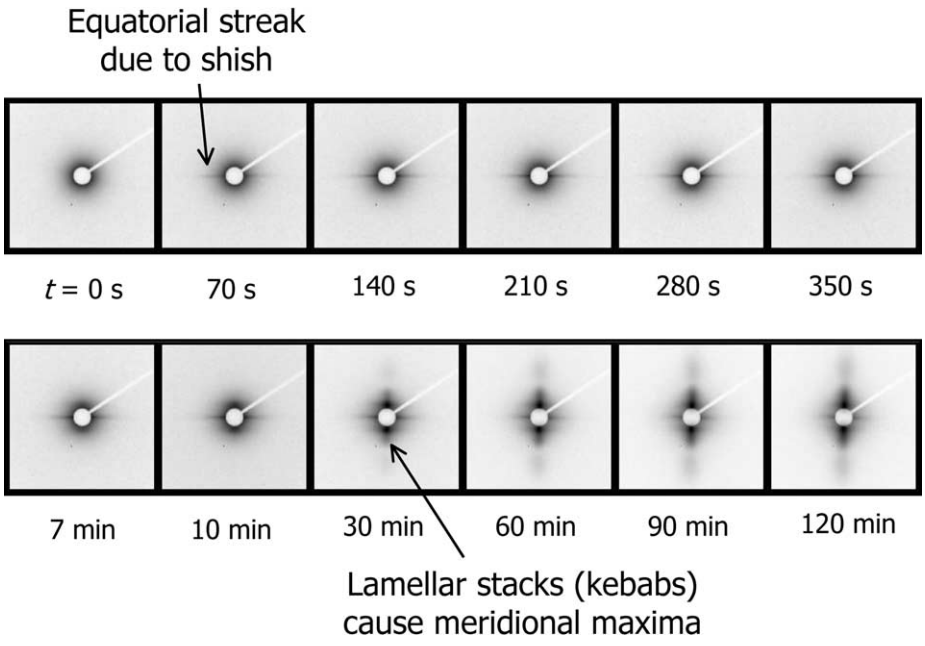

Fig. 6. 2D SAXS patterns of iPP melt before and at selected times after shear (shear rate = 60 s^{-1}, t_s = 5 s, T = 165 °C). [Reprinted with permission from Macromolecules 2002;35:9096. Copyright (2002) American Chemical Society].

under identical shear conditions. The patterns at the initial stages did not show any crystalline reflections. WAXD reflections from α-form iPP crystals appeared at a much later time (ca. 10 min) than the distinct scattering features observed in SAXS. At the final WAXD pattern (t = 120 min), four distinct reflections were observed at wavelength of 1.54 Å: (110) at $2\theta = 14.1°$, (040) at 16.9°, (130) at 18.5° and (−131) at 21.8° [53], all along the equator. These reflections were sharp and had narrow azimuthal width, indicating a highly oriented nature of iPP crystals, with good crystalline registration.

Although, no crystalline reflection was observed at the initial stages of crystallization, the immediate formation of shish-kebab morphology in the sheared melt was evident from the SAXS patterns in Fig. 6. This morphology indicates that the shish structure parallel to the flow direction is large enough to be detected by SAXS. From the shish, lamellae grow epitaxially and radially through the

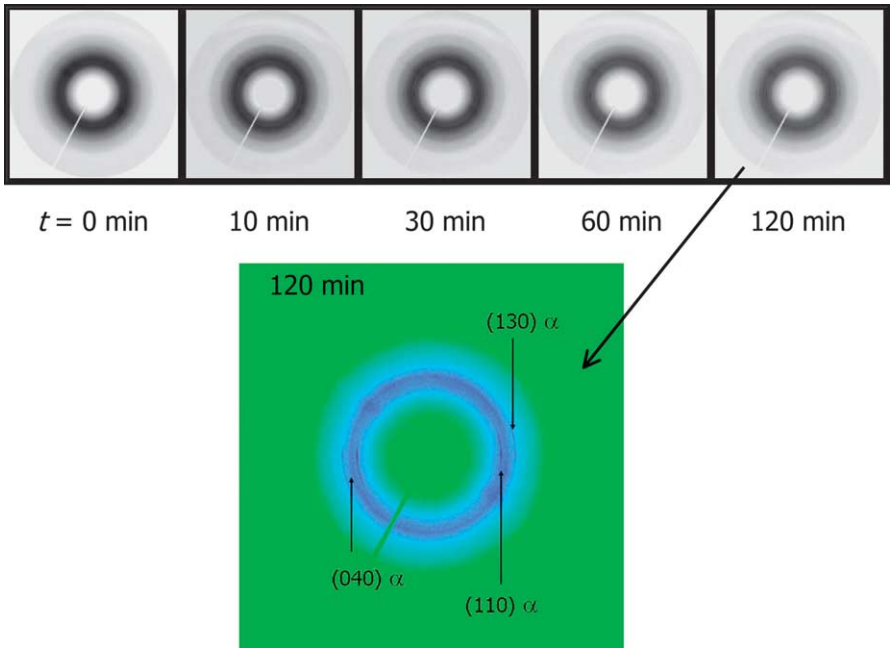

Fig. 7. 2D WAXD patterns of iPP melt before and at selected times after shear (shear rate = 60 s^{-1}, t_s = 5 s, T = 165 °C). [Reprinted with permission from Macromolecules, 2002;35:9096. Copyright (2002) American Chemical Society].

secondary nucleation process. On the other hand, WAXD patterns showed that the shish structure might not be crystalline at the early stages. To probe the nature (or its electron density via SAXS intensity) of the oriented shish-kebab structure at the early stages, a deconvolution procedure, called the 'Halo method' [114] was used to calculate the integrated SAXS intensity along the equator (I_{shish}) and meridian (I_{kebab}) and its trend with time after shear. Also, the time evolution of crystallinity was determined from the WAXD intensity profiles by a standard peak-fitting procedure [49,50].

The 2D SAXS pattern was deconvoluted into two components: (1) The isotropic part, due to scattering from the randomly distributed scatterers, and (2) the oriented part, originated by scattering from the oriented structures in the polymer melt (we avoid use of the word 'crystallites', since oriented structures formed at the initial stages may not be crystalline). The basic principle of the Halo method is as follows. The scattered intensity arising from the unoriented scatterers (isotropic) is azimuthal independent (a function of s only, where $s=2\sin\theta/\lambda$ is the scattering vector, and 2θ is the scattering angle), while the scattering arising from the oriented scatterers is azimuthal dependent (function of s and ϕ, where ϕ is the azimuthal angle). Accordingly, a series of azimuthal scans were drawn along the scattering vector starting from the center of the diffraction pattern. At each scattering vector s, a minimum scattering intensity value was obtained from the corresponding azimuthal scan. This minimum intensity was attributed to the isotropic scatterers, and deviation in the intensity along the azimuth was attributed to the oriented scatterers. The 2D image of intensity envelope obtained from the series of minimum values represents contribution from the unoriented scatterers. The 2D scattering image due to the oriented scatterers was then obtained after subtraction of the image corresponding to the isotropic component from the total scattered intensity image.

Values of I_{shish} and I_{kebab} were obtained by sectioning the SAXS pattern from the oriented shish-kebab scatterers observed in Fig. 6. Time evolution of I_{shish} and I_{kebab} are shown in Fig. 8(a) and (b), respectively. I_{shish} rose immediately after shear, whereas I_{kebab} increased only after a short induction time, about 210 s (inset of Fig. 8(b)). The initial rise of I_{shish} is the evidence of shish that consist of aligned chains, which provides the electron density contrast for the SAXS signal. The shish structure may not be crystalline, since there were no crystal reflections in WAXD patterns. It was seen that I_{shish} continuously increased even after cessation of shear. This may be due to the continuous ordering of chains in the mesomorphic shish or the linear growth of thin crystalline shish, where both structures could not result in distinct WAXD crystal reflections. Note that the shearing was stopped after 5 s, when the relaxation of polymer molecules had already begun. The shish growth was possible because motions of polymer chain segments in the shish structure were not yet restricted. These observations are consistent with the hypothesis of Petermann et al. [104,105], who argued that the shish growth can occur by an autocatalytically reproduced flow-field at the growth tip due to the free energy difference between the ordered structure and surrounding molecules; it does not necessarily require an external flow field. The increase in I_{shish} also implies that the connectivity between the linear precursors of nuclei along the flow direction significantly increases with time. As expected, the rate of increase in I_{shish} diminished at the later stage (Fig. 8(a)) due to relaxation of deformed polymer molecules in the melt.

On the other hand, I_{kebab} emerged after a short induction time and increased at a much greater rate than I_{shish}. It reached a significantly higher value, about 24 times higher at $t=120$ min after shear, than I_{shish}. The exact time of the emergence of meridional maxima after shear was determined from the Lorentz corrected 1D SAXS intensity profiles (Iq^2 versus q, where $q=2\pi s$) along the flow direction, as shown in Fig. 9. The location of the meridional intensity maximum can be clearly seen in these profiles; the magnified view of the SAXS intensity profiles at the early stages is shown in the inset of Fig. 9. The meridional maximum was first observed at $t=280$ s after shear. There is no doubt that the shish formed first and the kebabs formed later, consistent with the original model. The kebabs or folded-chain oriented crystals were initiated from the shish and grew perpendicularly to the flow direction forming layer-like lamellar structures. The spacing between the adjacent lamellar stacks was estimated to be about 600 Å. Typically the long spacing in semicrystalline iPP solid is in the range 200–300 Å at room temperature; the large spacing between the layers was an indication of a loosely packed precursor structure of kebabs at the early stages of crystallization.

3.1.1.3. Crystallinity development at 165 °C. Fig. 10 shows the linear WAXD intensity profiles taken from equatorial slices of the 2D WAXD patterns at selected times after shear, where the α-crystal reflection signals are the strongest. The (110) reflection of the α-crystals was observed only about 10 min after shear. Note that the sensitivity of the WAXD setup, as well as experimental conditions including sample thickness, will affect the exact time of emergence of crystal reflections; nevertheless, there were no crystals at the early stages or immediately after shear. The mass fraction of crystallites in the melt was estimated by a standard peak-fitting procedure of the WAXD intensity profile. At $t=120$ min after shear, the estimated value of the crystallinity was only about 2.3%. The low crystallinity was due to the following reason. Since the experimental temperature (165 °C) was near the nominal melting point of iPP crystals, only the shear-induced oriented crystals, which were stable at the high temperature, contributed to the crystallinity. The SAXS and WAXD patterns at $t=120$ min after shear clearly suggested that the sheared melt consisted mostly of oriented crystals.

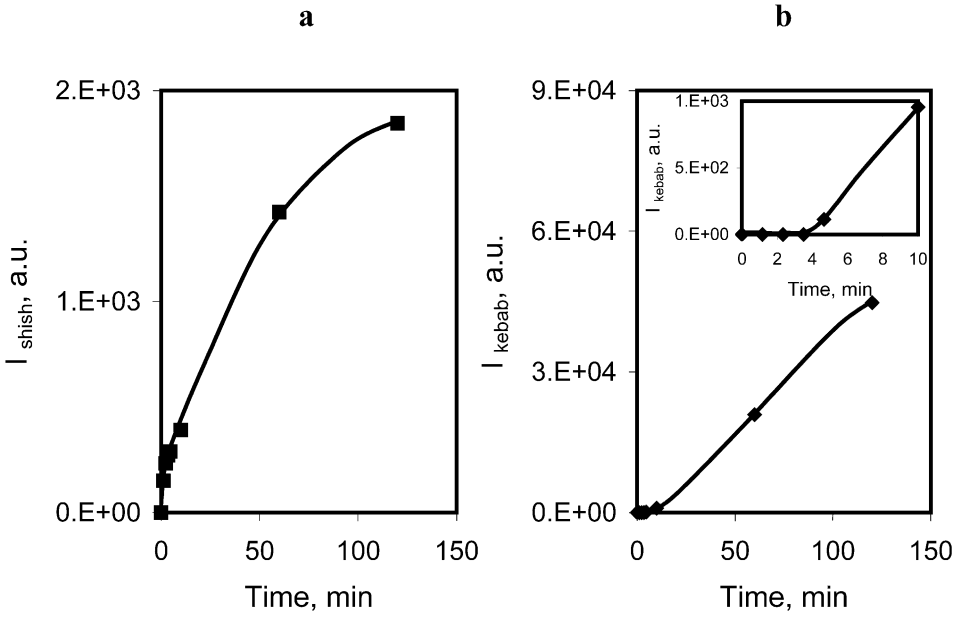

Fig. 8. Time evolution of SAXS integrated intensities, (A) I_{shish} and (B) I_{kebab} after shear (shear rate = 60 s^{-1}, t_s = 5 s, T = 165 °C). [Reprinted with permission from Macromolecules 2002;35:9096. Copyright (2002) American Chemical Society].

3.1.1.4. Melting temperature of the shish-kebab structure in iPP. As mentioned in Section 2.2, in the early studies of PE shish-kebab structure, it was found that shish were highly stable to the point that they could be superheated; their melting temperature was about 15–20 °C higher than PE spherulites or lamellae [101]. Therefore, it was believed that the shish was formed by crystallization of fully extended chains. We determined the difference in the melting point temperature of the shish-kebab structure (the oriented crystals), and spherulites (the unoriented crystals) in iPP by two methods; in situ SAXS and DSC. After completion of rheo-SAXS experiment at 165 °C, the iPP sample was rapidly cooled to room temperature. The sample was then heated from room temperature until the shish and kebabs melted away, while continuously acquiring 2D SAXS images. In another duplicate experiment, the sheared sample was preserved for DSC study. Figs. 11 and 12 show in situ SAXS patterns at selected temperatures and corresponding DSC thermograms, respectively. These results clearly showed that the unoriented iPP crystals melted at about 165 °C. The kebabs started to melt at about 170–175 °C, while the shish completely melted at about 180–185 °C. The melting temperature of the shish was about 5–10 °C higher than the kebabs and about 15–20 °C higher than the spherulites. Although the higher melting temperature of shish is related to the underlying chain conformation in its structure, it does not necessarily indicate that the chains in shish are fully extended. However, it certainly indicates a

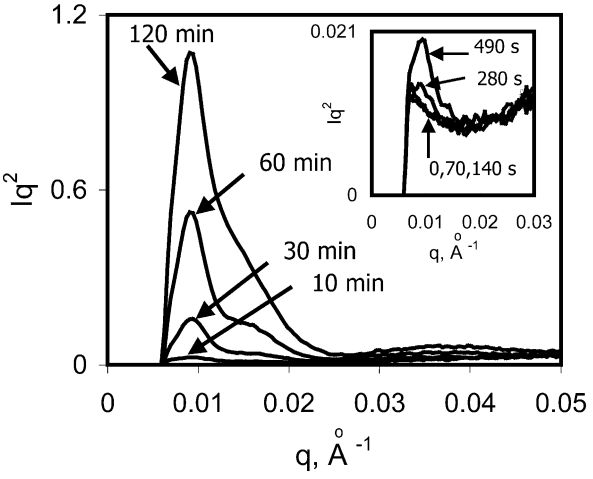

Fig. 9. Lorentz corrected SAXS intensity profiles along the meridian; the inset shows profiles (magnified) at the early stages after shear (shear rate = 60 s^{-1}, t_s = 5 s, T = 165 °C). [Reprinted with permission from Macromolecules 2002;35:9096. Copyright (2002) American Chemical Society].

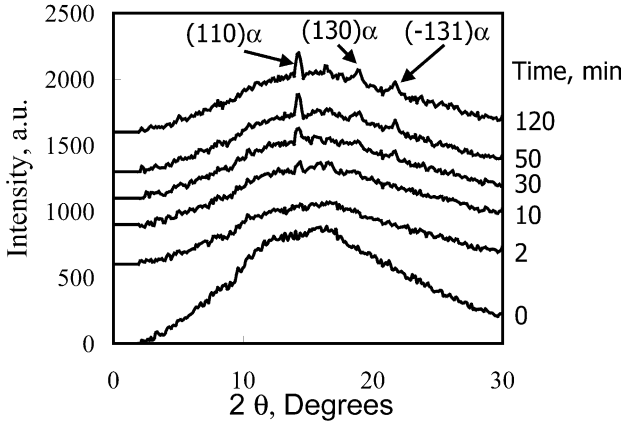

Fig. 10. 1D WAXD intensity profiles along the equator at selected times after shear (shear rate = 60 s^{-1}, t_s = 5 s, T = 165 °C). [Reprinted with permission from Macromolecules 2002;35:9096. Copyright (2002) American Chemical Society].

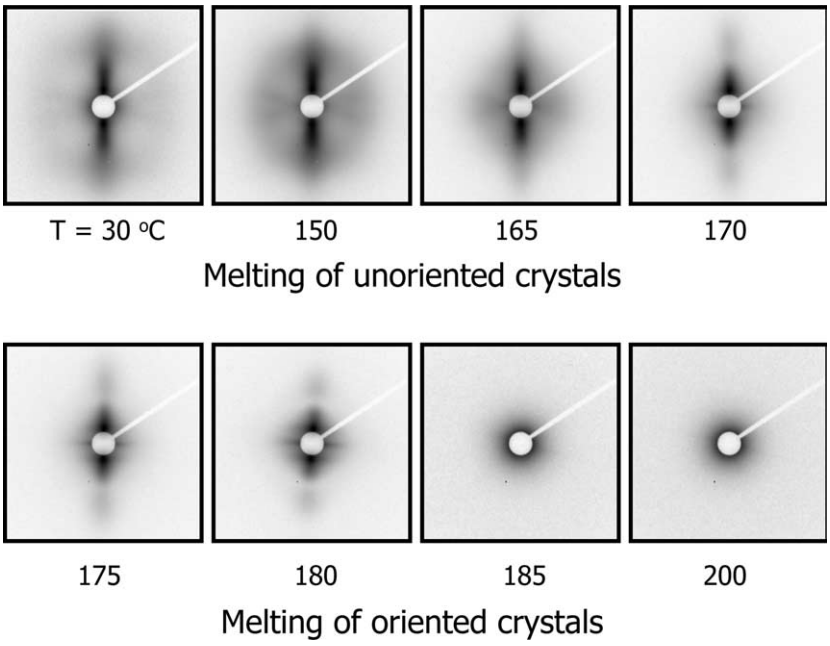

Fig. 11. 2D SAXS patterns at selected temperatures during heating of a sheared iPP sample (shear rate = 60 s^{-1}, t_s = 5 s), showing melting temperatures of the unoriented and shear-induced oriented crystals.

linear connectivity of the chains in the shish that results in its long length (high crystal thickness) and, hence, its higher melting point than the spherulites.

3.1.2. Blend of iPP and atactic polypropylene

In this study [54], we investigated the feasibility of having a shear-induced precursor structure, which is non-crystalline and non-mesomorphic, by using high molecular weight amorphous atactic polypropylene (aPP) as the precursor component in a low molecular weight crystalline iPP matrix. The chosen samples were as follows: High molecular weight aPP (M_n = 256,000 g/mol, M_w = 670,000 g/mol, M_z = 1,290,000 g/mol) and relatively low molecular weight iPP (M_n = 55,000 g/mol, M_w = 127,000 g/mol, M_z = 230,000 g/mol). A solution blending procedure was used to prepare the blend of 95:5 wt% iPP/aPP, which

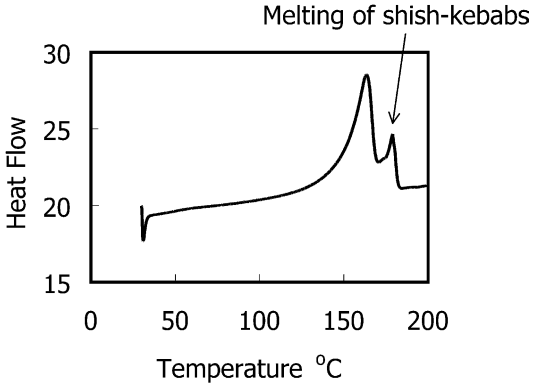

Fig. 12. DSC thermogram of sheared iPP sample (shear rate = 60 s^{-1}, t_s = 5 s). [Reprinted with permission from Macromol Symp 2002;185:105. Copyright (2002) Wiley-VCH Verlag GmbH and Co. KGaA, Weinheim].

ensured mixing of the two components at the molecular level. Our rationale was as follows. The aPP chain segments are not likely to be incorporated in the iPP crystal, owing to the stringent requirement of the crystal stem concerning the pending CH_3 groups. If aPP molecules, which do not crystallize, aid in the formation of iPP nucleation, it is an indication that the iPP nuclei can originate from a precursor structure that possesses oriented and extended amorphous chains. This will be consistent with the simulation results of Frenkel et al. [29], who demonstrated that even a single aligned chain can act as a 'template' for crystallization of kebabs. Recently, Lotz [115] proposed a stem-by-stem deposition process for polymer crystal growth under quiescent conditions. Accordingly, crystallization of chiral but racemic polymers (e.g. iPP), in which the building units of the crystal are short helical stems, is a highly sequential and substrate-determined process, i.e. the depositing stem probes the topography of the growth face prior to attachment. Lotz hypothesized that the primary nucleus at the initial stage could be a small entity, perhaps an individual stem. If this situation exists in flow, that is, if primary nuclei at the initial stages were an individual helical stem (oriented chain segment of iPP) then the depositing stems must satisfy the stringent criterion of chain segment conformation. Only oriented chain segments of iPP molecules can satisfy this requirement, as stems of aPP molecules do not, and their addition should not affect the degree of orientation and crystallization kinetics. In another scenario, if primary nuclei at the initial stages were spontaneously formed tiny crystals, then the addition of aPP molecules that do not crystallize and cannot be incorporated in iPP crystals, should not affect the nucleation

and corresponding kinetics of iPP. The experimental results of the iPP/aPP blend were not in agreement with either of the above scenarios. Instead, the results clearly showed that the primary nuclei of shish/kebab originated from a flow-induced precursor structure that is non-crystalline.

Fig. 13(a) and (b) shows 2D rheo-SAXS and -WAXD patterns; respectively, of the pure iPP melt and iPP/aPP blend at 60 min after cessation of shear (shear rate = 60 s^{-1}, duration of shear, $t_s = 5$ s, $T = 145$ °C). The SAXS patterns showed that the intensity of the meridional maxima arising from the oriented lamellae stacks or kebabs was significantly stronger in the case of blend compared to pure iPP. Note that in SAXS patterns of the iPP and iPP/aPP blends, meridional maxima were superimposed on a diffused scattering ring due to the unoriented crystals. Note that no equatorial reflections were detected in the SAXS patterns, which indicated that the extended-chain shish were tiny and farther apart (if crystalline), or that they were non-crystalline with little or no electron density contrast against the surroundings. We note that size of the beamstop in SAXS setup limited the detection of the scattering signal at very low angles. Since shish entities grew very rapidly, the scattering signal due to shish or equatorial streaks might move inside the beamstop, and could not be detected.

The corresponding WAXD patterns showed that, the degree of iPP crystal orientation was significantly higher in the blend compared to that in a pure component. In the case of the blend, the azimuthal breadths in the intensity of the α-crystal reflections (e.g. (110) and (040) reflections) were relatively narrow, a signature of the high degree of crystal orientation; while it was relatively weak in the case of pure iPP.

Fig. 14 shows time evolution of the total crystalline iPP phase in pure iPP and iPP/aPP blend at 145 °C. A typical

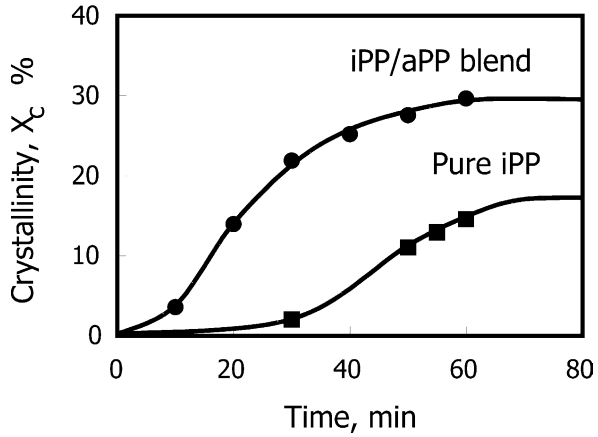

Fig. 14. Time evolution of the total percent crystallinity in the pure iPP and iPP/aPP (5 wt%) blend at 145 °C after shear (shear rate = 60 s^{-1}, $t_s = 5$ s). [Reprinted with permission from J Macromol Sci, Phys 2003;B42(3–4): 515. Copyright (2003) Macel Dekker Inc.].

polymer crystalline phase growth profile was obtained. It was seen that for both systems, the volume fraction of the total crystallinity increased with time and subsequently reached a plateau value. The half-time of crystallization ($t_{1/2}$) was determined from the plot of relative crystallinity ($X_r = X_c(t)/X_c(\infty)$) versus time, where X_r is the relative crystallinity, $X_c(t)$ is the total crystallinity at time t, and $X_c(\infty)$ is the steady state value (plateau value) of the total crystallinity. The half-time of crystallization was determined as the time at which the relative crystallinity reached a value of 0.5. The estimated value of $t_{1/2}$ for the blend was 21 min compared to 45 min for pure iPP. We concluded that the iPP/aPP blend crystallized much faster than pure iPP.

The results of these experiments clearly showed that the addition of higher molecular weight aPP (i.e. with long

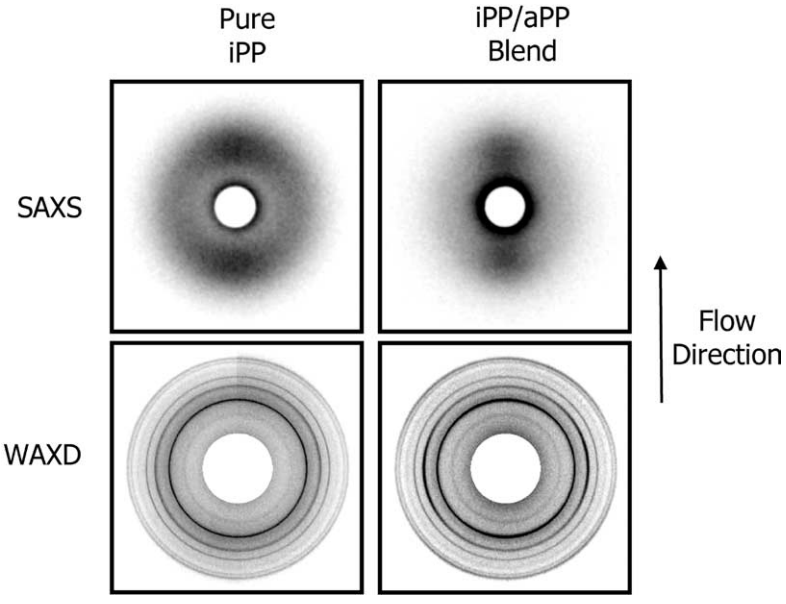

Fig. 13. 2D SAXS and WAXD patterns of the pure iPP and iPP/aPP (5 wt%) blend 60 min after cessation of shear (shear rate = 60 s^{-1}, $t_s = 5$ s, $T = 145$ °C). [Reprinted with permission from J Macromol Sci, Phys 2003;B42(3–4):515. Copyright (2003) Macel Dekker Inc.].

chain lengths and long relaxation times) affected both the extent of orientation and crystallization kinetics of the lower molecular weight iPP matrix. The degree of iPP crystal orientation was significantly higher (Fig. 13) and its crystallization kinetics substantially improved (Fig. 14) in the iPP/aPP blend. These observations indirectly indicated the presence of a shear-induced precursor scaffold, containing long amorphous aPP chains as non-detectable shish and short iPP crystals as kebabs, which aided in secondary nucleation and thus the crystallization kinetics of the surrounding iPP matrix. Therefore, the flow-induced precursor structure can indeed contain oriented, stretched but non-crystalline chains as shish.

3.1.3. Effects of flow intensity on shish-kebab formation

In this section, the studies and results of how the total flow intensity affected the formation and characteristics of the shish-kebab structures is presented [57]. The same Ziegler–Natta iPP polymer sample (characteristics given in Section 3.1.1) was used in these experiments. As mentioned in Section 2.1, according to the concept of coil–stretch transition and the original theme of Keller's work, for polydispersed solution and melts in elongational flow, increasing $\dot{\varepsilon}$ does not affect the degree of chain extension (since only either random coil or fully extended conformation is possible), but will increase the amount of material that becomes extended by increasingly cutting into the distribution from the high molecular weight tail downwards (Fig. 2). The above is presumed to be applicable in the case of shear or mixed flow conditions as well; despite the fact that, shear flow has a strong rotational component. The recent dilute solution experiments of Chu et al. [32] showed that, in steady-state shear, the mean fractional extension increased gradually with imposed flow strength; characterized by the Weissenberg number, *Wi*, and it approached an asymptotic value of only 0.4–0.5. They noted that this behavior differs markedly from the behavior observed in pure elongational flow, where molecular extension rises rapidly to a value close to the full contour length of the chain at relatively low deformation rates (Fig. 15). The Weissenberg number, *Wi*, is the ratio between the flow time scale (reciprocal shear rate) and the diffusion time scale (the longest relaxation time), accounting for Brownian motion-induced conformation changes. The corresponding situation in an entangled melt is more complex due to inter- and intra-molecular interactions. Intuitively, polymer chain dynamics is expected to be affected by the characteristics of the surrounding matrix, such as viscosity, mesh size and chain length between the entanglement points. How these variables affect the early stage events in the deformed melt and subsequent crystalline morphology or microstructure is not clear.

Our approach to these studies can be summarized as follows. Based on the works of Keller [1] and Lotz [115], we propose that there is a two-way connection between the degree of molecular orientation in flow and the crystal morphology resulting there from. That is, quantification of the orientation in the melt at high temperatures, even after cessation of shear, and of the oriented crystal fractions in the fully crystallized sample at room temperature can serve as a pointer to the pre-existing state of molecular extension/orientation in the deformed melt. The results revealed that both the degree of crystal orientation (Herman's orientation function, *f*) in the melt at 165 °C and the oriented crystals fraction (X_o) in the fully crystallized sample increased with shear rate as well as with shear duration. Interestingly, at a constant total strain, short duration shear at high rate was more effective in orientating molecules in flow than long duration shear at low rate. Also, Both *f* and X_o were found to gradually increase with increasing flow intensity or *Wi*, and approached a plateau value at high values of *Wi*. Thus, we concluded that even under a very intense shear field (or high *Wi*) all polymer molecules do not extend to the full contour length, and that the average chain extension has a limiting value, much below the fully extended chain length.

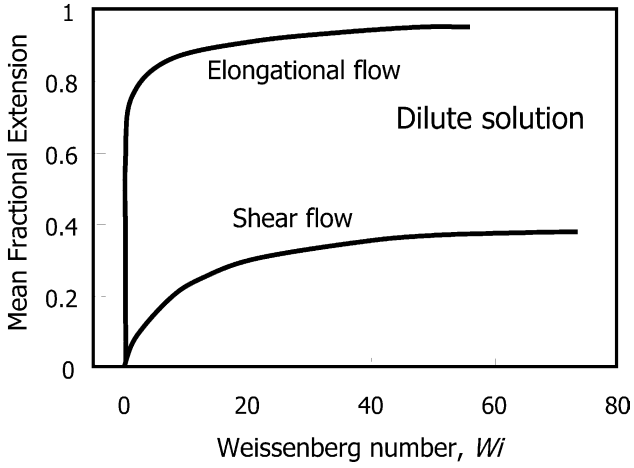

Fig. 15. The effect of flow intensity or Weissenberg number, *Wi* on the mean fractional extension of molecules in dilute solution under shear and elongational flow. [Reprinted with permission from Science 1999;283: 1724. Copyright (1999) The American Association for the Advancement of Science].

Fig. 16 shows 2D SAXS and WAXD patterns of iPP melt at 165 °C obtained 60 min after cessation of shear at shear rates of 30, 45 and 60 s^{-1} (shear duration was constant, t_s = 5 s). The corresponding SAXS and WAXD patterns of fully crystallized samples at room temperature are shown in Fig. 17. SAXS and WAXD patterns of iPP melt at 165 °C obtained 60 min after cessation of shear for shear durations of 1.3, 3 and 5 s (shear rate constant, rate = 60 s^{-1}) are shown in Fig. 18, and those of the fully crystallized sample are shown in Fig. 19. The SAXS and WAXD images in Figs. 16–19 exhibited qualitative evidence of the flow intensity effects, as expected. It was seen that both SAXS and WAXD intensities due to the oriented crystals increased with shear rate (at a constant shear duration) as well as with shear duration (at a constant shear rate). Interestingly, these patterns revealed that, at a constant strain, the degree of

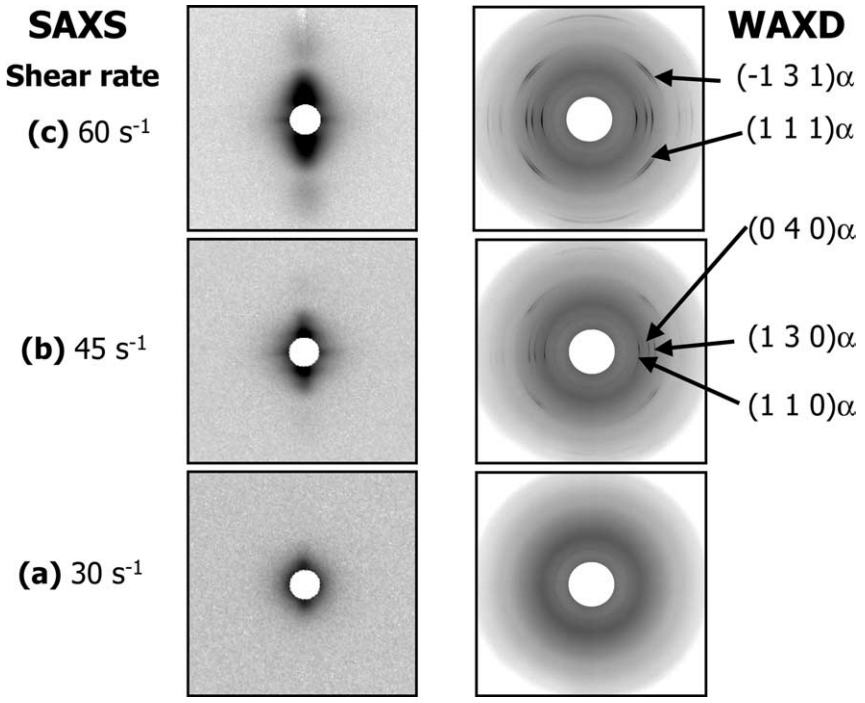

Fig. 16. 2D SAXS and WAXD images of iPP melt 60 min after cessation of shear at different shear rates: (a) 30 s^{-1}, (b) 45 s^{-1} and (c) 60 s^{-1} (shear duration = 5 s and T = 165 °C). [Reprinted with permission from Macromolecules 2005; in press. Copyright (2005) American Chemical Society].

crystal orientation and oriented crystal fractions were higher in short duration shear at high shear rate than those in long duration shear at low shear rate. For example, the SAXS and WAXD intensity at a shear rate of 60 s^{-1} and t_s = 1.3 s (strain = 78) was stronger than that at shear rate of 30 s^{-1} and t_s = 5 s (strain = 150). Similarly, the intensity was stronger at shear rate of 60 s^{-1} and t_s = 3 s (strain = 180) than that at 45 s^{-1} and t_s = 5 s (strain = 225).

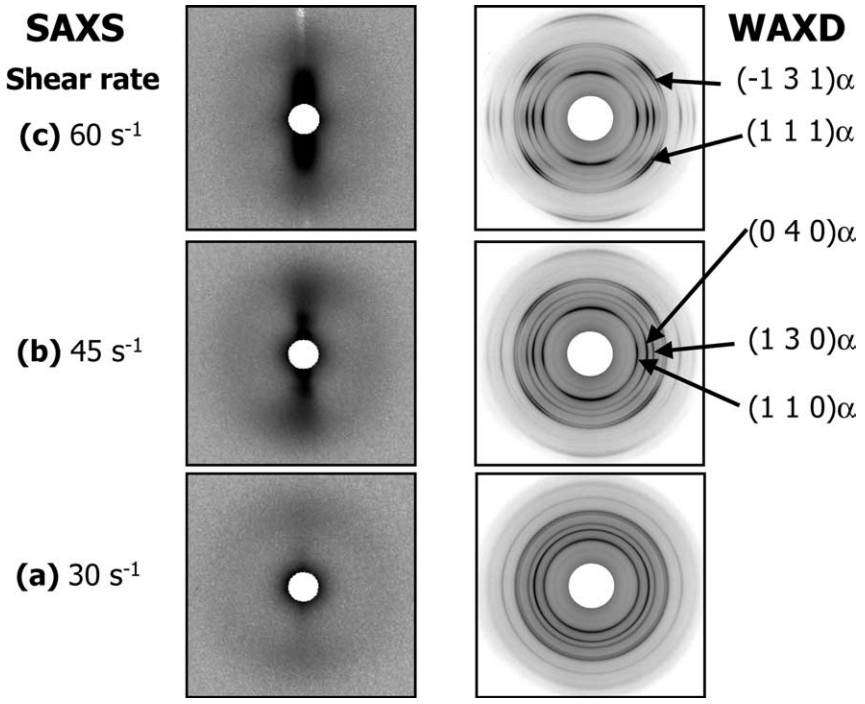

Fig. 17. 2D SAXS and WAXD images of sheared iPP polymer at room temperature. Note that sheared melt was kept at 165 °C for 1 h after cessation of shear, and then cooled to room temperature. At different shear rates: (a) 30 s^{-1}, (b) 45 s^{-1} and (c) 60 s^{-1} (shear duration = 5 s). [Reprinted with permission from Macromolecules, 2005; in press. Copyright (2005) American Chemical Society].

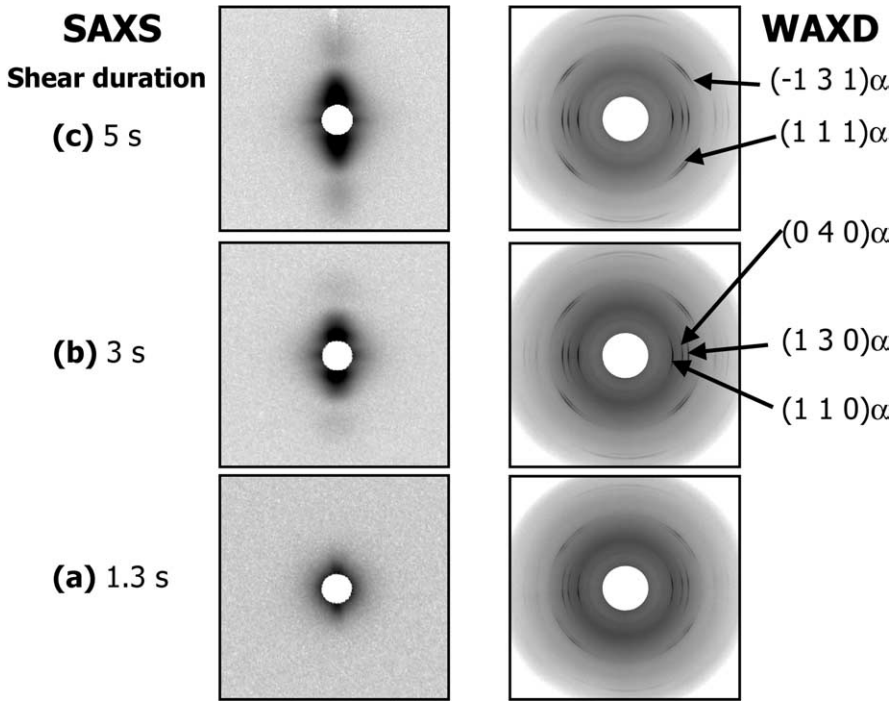

Fig. 18. 2D SAXS and WAXD images of iPP melt 60 min after cessation of shear at different shear duration: (a) 1.3 s, (b) 3 s and (c) 5 s (shear rate = 60 s^{-1} and $T = 165$ °C). [Reprinted with permission from Macromolecules 2005; in press. Copyright (2005) American Chemical Society].

3.1.3.1. Degree of crystal orientation in sheared iPP Melt at 165 °C. Quantitatively, the degree of crystal orientation in the sheared iPP melt was determined by using the Herman's method [116]. Accordingly, the crystalline orientation can be characterized by average orientation of the normal to the crystalline plane with respect to an external reference frame. Here, the flow direction was taken as the reference direction. For a set of *hkl* planes, the average orientation, expressed as

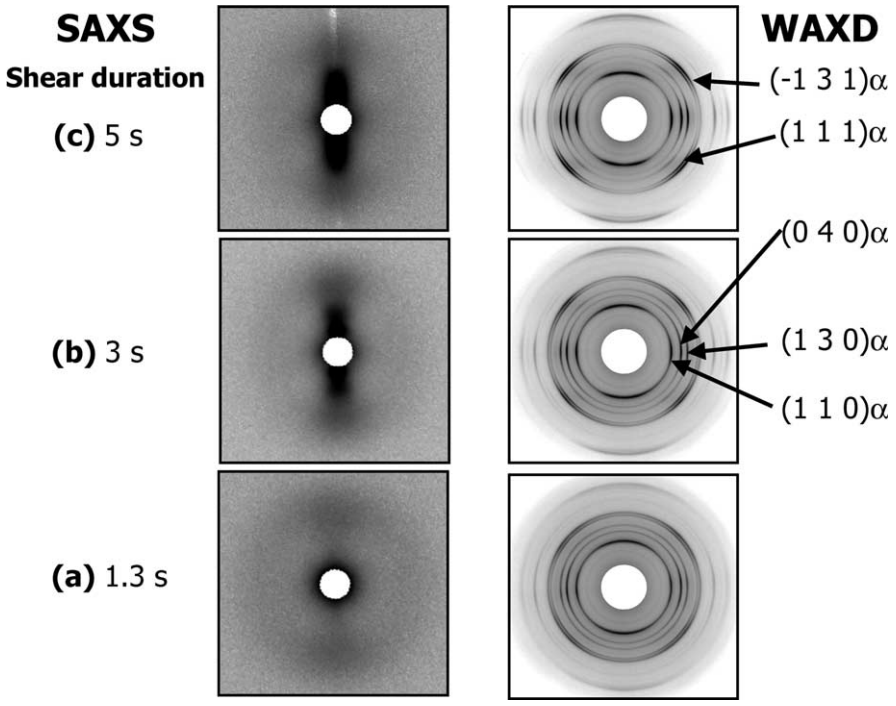

Fig. 19. 2D SAXS and WAXD images of sheared iPP polymer at room temperature. Note that sheared melt was kept at 165 °C for 1 h after cessation of shear, and then cooled to room temperature. At different shear duration: (a) 1.3 s, (b) 3 s and (c) 5 s (shear rate = 60 s^{-1}). [Reprinted with permission from Macromolecules 2005; in press. Copyright (2005) American Chemical Society].

$\langle\cos^2\phi\rangle_{hkl}$, can be calculated mathematically using the following equation:

$$\langle\cos^2\phi\rangle_{hkl} = \frac{\int_0^{\pi/2} I(\phi)\cos^2\phi \sin\phi \mathrm{d}\phi}{\int_0^{\pi/2} I(\phi)\sin\phi \mathrm{d}\phi} \quad (1)$$

where ϕ is the azimuthal angle and $I(\phi)$ is the scattered intensity along the angle ϕ. Herman's orientation function, f, is defined as

$$f = \frac{3\langle\cos^2\phi\rangle_{hkl} - 1}{2} \quad (2)$$

where f has the value of -0.5, when the normal of the reflection plane is perpendicular to the reference direction ($\phi = 90°$ or crystals are oriented parallel to the flow direction), a value of 1, when the normal is parallel to the reference direction ($\phi = 0°$ or crystals are oriented perpendicularly to the flow direction), and a value of 0, when the orientation is random. The degree of orientation was calculated from the azimuthal intensity distribution, $I(\phi)$, of the strongest (110) reflection of α-crystals at $2\theta = 14.1°$.

Figs. 20 and 21 show the value f (at $t = 60$ min after shear) as a function of shear rate and shear duration, respectively. The most interesting aspect of these results was that f appeared to approach a plateau value at high shear rate, or high shear duration. Subsequently, how this affects the final fully crystallized polymer microstructure, i.e. the oriented crystal fraction, was found to be an indicator of the pre-existing molecular orientation in the deformed melt at the early stages.

3.1.3.2. Oriented crystal fraction in fully crystallized iPP. The fraction of oriented scatterers in the sheared iPP sample detected by SAXS was determined using the Halo method with the following procedures. The fraction of oriented scatterer, which was proportional to the oriented crystal fraction by WAXD, was defined as the ratio of integrated

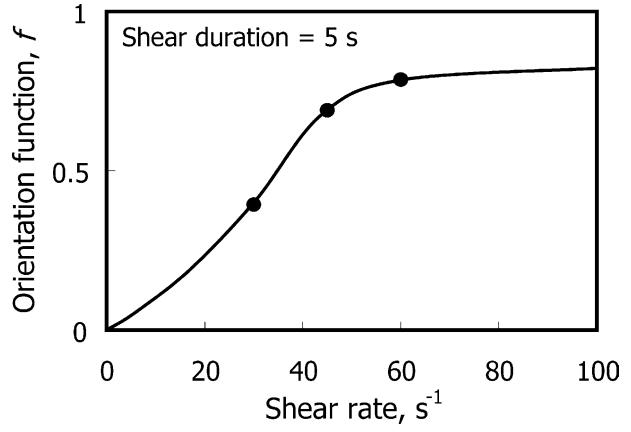

Fig. 20. Herman's orientation function, f, at 1 h after cessation of shear as a function of shear rate (shear duration = 5 s and $T = 165$ °C). [Reprinted with permission from Macromolecules 2005; in press. Copyright (2005) American Chemical Society].

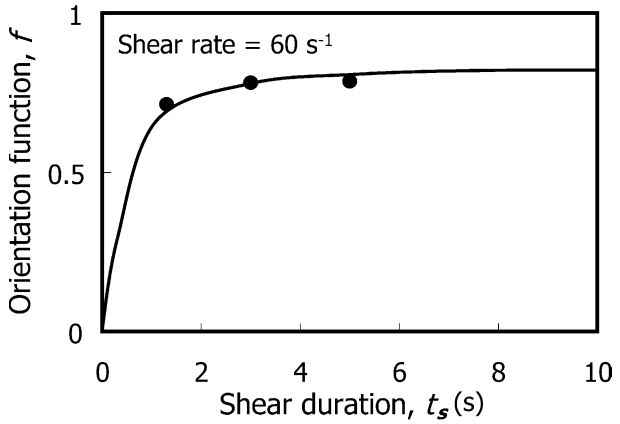

Fig. 21. Herman's orientation function, f, at 1 h after cessation of shear as a function of shear duration (shear rate = 60 s^{-1} and $T = 165$ °C). [Reprinted with permission from Macromolecules 2005; in press. Copyright (2005) American Chemical Society].

SAXS intensity due to the oriented structures, $I_{oriented}$, and total integrated SAXS intensity, I_{total}. The total percent crystallinity (X_t) and crystallinity due to the oriented (X_o) and unoriented (X_u) crystals were obtained from the WAXD patterns. Fig. 22 shows the values of X_t, X_o and X_u, of the sheared iPP sample at room temperature as a function of shear rate. The calculated values of oriented fraction (SAXS) are also shown in Fig. 22 (each data point is illustrated as an asterisk). Similarly, the values of these parameters as a function of shear duration are presented in Fig. 23. The main features of Figs. 22 and 23 were as follows: (1) The final total crystallinity (53–57%) was constant under all shear conditions, (2) the crystallinity due to oriented crystals (WAXD) and oriented fraction (SAXS) increased with shear rate as well as with shear duration, and (3) the crystallinity due to oriented crystals reached a plateau value at high shear rates as well as at high shear durations. Theoretically, the plateau value is bound by the value of total crystallinity.

The orientation function represents the average degree of crystal orientation in the sheared iPP melt at 165 °C and must be directly related to the mean orientation/extension of the polymer molecules. This may be reasoned as follows. All crystallizable species in the sheared melt crystallize upon cooling. The surface of already formed oriented crystals acts as nuclei for the crystallizing species; the melt that has a greater number of nuclei will result in a higher degree of the oriented crystals (X_o) in the crystallized polymer. Thus, the oriented crystals fraction at room temperature is a signature of the extent of molecular orientation developed in flow. The results indicated a limiting value for the mean molecular orientation/extension, even at intense shear flow conditions.

3.1.3.3. Weissenberg number and molecular orientation. To obtain quantitative estimates of the Weissenberg number,

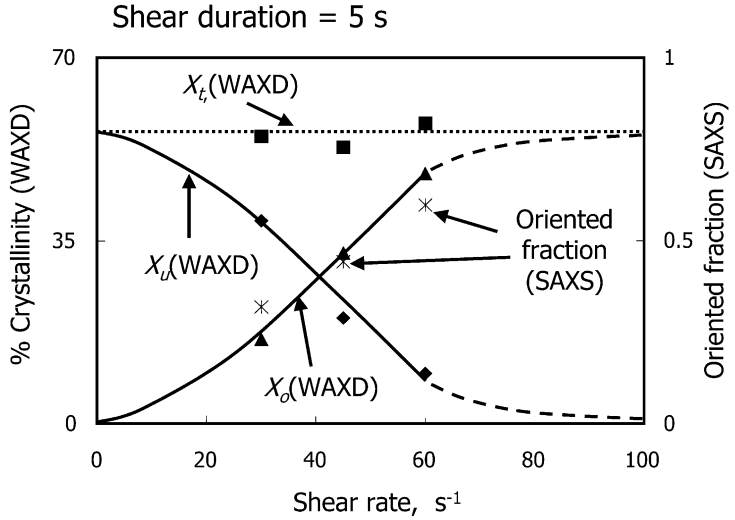

Fig. 22. The percent crystallinity (WAXD); total, due to the oriented and unoriented crystals, and oriented fraction from SAXS (the data in asterisk) of the fully crystallized polymer at room temperature as a function of shear rate (constant shear duration = 5 s). [Reprinted with permission from Macromolecules 2005; in press. Copyright (2005) American Chemical Society].

the longest relaxation time at the experimental temperature of 165 °C was estimated from the rheological data, i.e. dynamic moduli, $G'(\omega)$ and $G''(\omega)$ that were measured in small amplitude oscillatory shear experiments. Horizontal temperature shift factors, a_T, were calculated from the data at several temperatures. The discrete relaxation time spectrum for the iPP sample was determined by non-linear regression fit of the G' and G'' master curves at the reference temperature of 140 °C, shown in Fig. 24. The longest relaxation time, λ_{max} (=70 s), was taken as the time when the relaxation strength drops by more than two orders of magnitude. The λ_{max} versus temperature relationship was estimated from the horizontal shift factors; the calculated curve is shown in Fig. 25. Thus, λ_{max} for the iPP sample at 165 °C is about 34.5 s.

Fig. 26 shows values of f and X_o versus Wi. As expected, both f and X_o reached plateau values at high Wi. We expect a similar trend for the mean molecular extension/orientation as a function of Wi. In other words, as in the case of dilute polymer solutions, the mean molecular extension in an entangled polymer melt gradually increases with Wi and reaches a plateau value at high values of Wi. The magnitude of plateau value of mean molecular extension in shear is probably significantly lower than the chain contour length. Based on the work of Chu et al. [32], this may be because of the following reasons. Shear flow has both extensional and

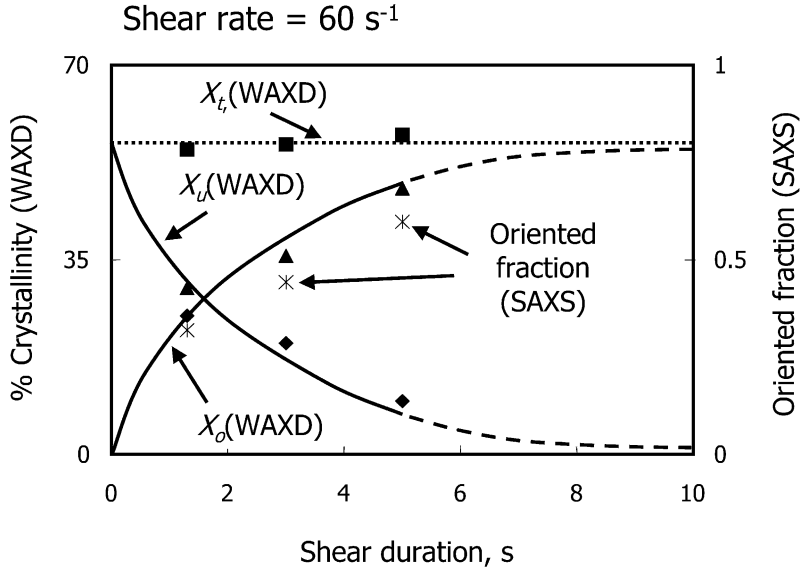

Fig. 23. The percent crystallinity (WAXD); total, due to the oriented and unoriented Crystals, and oriented fraction from SAXS (the data in asterisk) of the fully crystallized polymer at room temperature as a function of shear duration (constant shear rate = 60 s^{-1}). [Reprinted with permission from Macromolecules 2005; in press. Copyright (2005) American Chemical Society].

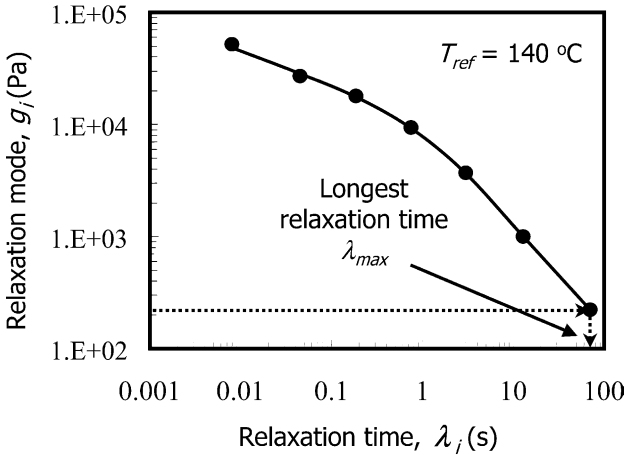

Fig. 24. Discrete relaxation spectrum and the longest relaxation time of iPP polymer at the reference temperature of 140 °C.

rotational components. The extensional components orient and/or stretch polymer molecules. The rotational components cause end-over-end tumbling and the stretched state is destabilized. Thus, molecules stretch, tumble, and retract in a stochastic manner. Since, both the stretching and tumbling components are driven by the velocity gradient, the random stretching and contraction process occurs more frequently at higher shear rates. Thus, in an entangled melt, mean molecular orientation/extension that can be achieved in shear should be much lower than the full contour length even at high values of *Wi*.

3.1.4. Model polyethylene blends

In other complementary studies [56], in situ rheo-SAXS experiments were performed with specifically designed bimodal polyethylene (PE) blends. In these blends, the matrix consisted of a relatively low molecular weight component and was kept amorphous during the experiment; the minor component was a high molecular weight, miscible and crystallizing component. These blends simulate a

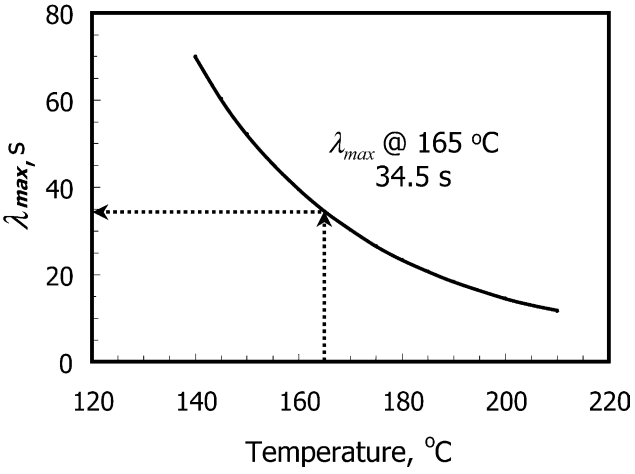

Fig. 25. The longest relaxation time of the iPP polymer as a function of temperature.

'dilute polymer solution' condition, and thus allow examination of the crystallization behavior of only the high molecular weight species under flow. Moreover, the chosen experimental temperature was such that crystallization kinetics of the high molecular weight species was sufficiently slow (the transition period in minutes instead of seconds), which enabled us to probe the molecular processes during the formation of precursor structures (shish-kebabs) under flow.

In the first study [56], two series of blends were prepared; low molecular weight PE copolymers (2% hexane) with weight-average molecular weights of 50,000 and 100,000 g/mol, designated as MB-50k and MB-100k, respectively, were used as the 'solvent' component or the matrix material. A high molecular weight PE homopolymer with M_w of 250,000 g/mol (MB-250k), miscible with both low molecular weight PE matrices, was selected as the crystallizing component. The end of the melting zone ($T_{m,end}$ in DSC thermogram) of the low molecular weight component was chosen as the experimental temperature. The concentrations of the binary blends (3, 5 and 10 wt%) were above the overlap concentration, C^* (based on the published data for 250k linear PE, its C^* was about 1 wt%), thus ensuring the entangled polymer melt situation. All blends were prepared by a solution blending procedure that ensured intimate mixing at the molecular level.

3.1.4.1. MB-50k/MB-250k and MB-100k/MB-250k blends.

Fig. 27 shows selected 2D WAXD patterns of the MB-100k/MB-250k blend at (a) 95/5 and (b) 90/10 compositions at different times after shear (shear rate = 60 s^{-1}, shear time = 5 s, T = 120 °C). Note that the experiments of pure MB-100k polymer with shear and without shear as well as the MB-100k/MB-250k (90/10) blend without shear were first carried out to confirm that no crystallization took place under these conditions. In shear experiments, the blends showed that crystal orientation and crystallization kinetics increased significantly after shear with the increase in the MB-250k concentration. The overall behavior of the MB-100k/MB-250k (95/5) blend (Fig. 27(a)), exhibiting the occurrence of four (110) peaks at the off-axis positions due to the formation of twisted lamellae [1,56], was similar to that of the MB-100k/MB-250k (97/3) blend. In contrast, the WAXD pattern of the MB-100k/MB-250k (90/10) blend obtained immediately after shear (~30 s) showed a very unique feature. It was found that a pair of sharp (110) reflections appeared almost immediately upon the cessation of flow on the equator (Fig. 27(b)). The formation of this equatorial two-spot pattern at the very early stages of crystallization indicated that the first formed crystals had a very high orientation and the chains in the formed crystals were aligned parallel to the flow direction. As the crystallization progressed, a composite pattern having six (110) reflections and two (200) reflections in the meridian (as seen the 135 and 285 s SAXS patterns in Fig. 28(b)) was observed. Note that the overall behavior of the MB-50k/

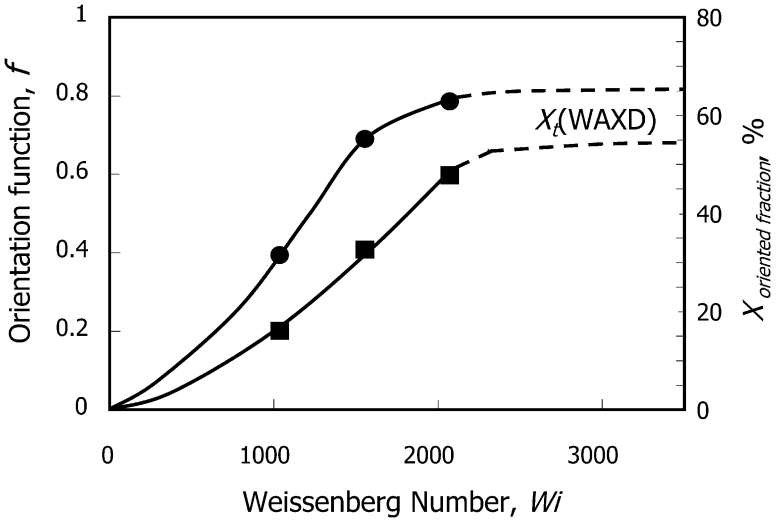

Fig. 26. Herman's orientation function, f (as shown in filled circle), of the sheared melt (at 165 °C and 1 h after shear), and the crystallinity due to oriented crystals, X_o (as shown in filled square), of the crystallized polymer at room temperature as function of Weissenberg number, Wi. [Reprinted with permission from Macromolecules 2005; in press. Copyright (2005) American Chemical Society].

MB-250k blend was quite similar to that of the MB-100k/MB-250k (95/5) blend (Fig. 28(a)), except that it showed a faster crystallization rate compared to its counterpart.

2D SAXS patterns of (a) MB-100k/MB-250k (95/5) and (b) MB-100k/MB-250k (90/10) blends at selected times after shear (shear rate = 60 s^{-1}, shear time = 5 s, T = 120 °C) are shown in Fig. 28. Again, SAXS measurements of pure the MB-100k polymer under shear and no shear as well as of the MB-100k/MB-250k (90/10) blend under no shear were carried out. All SAXS patterns of MB-100k obtained during the experimental time frame of 45 min exhibited no scattering profile. SAXS patterns of the MB-100k/MB-250k (90/10) blend under no shear exhibited a scattering ring with no preferred orientation, indicative of the formation of only randomly distributed lamellar structures. The development of oriented superstructures was observed in both MB-100k/MB-250k (95/5) and MB-100k/MB-250k (90/10) blends after shear. The behavior of MB-100k/MB-250k (95/5) was similar to that of a typical polymer melt in shear. A pair of weak meridional scattering maxima appeared at 285 s after shear; the subsequent SAXS patterns showed the growth of the meridional maxima with time (not shown here), due to the formation of well-recognized lamellar layered structures of MB-250k crystals

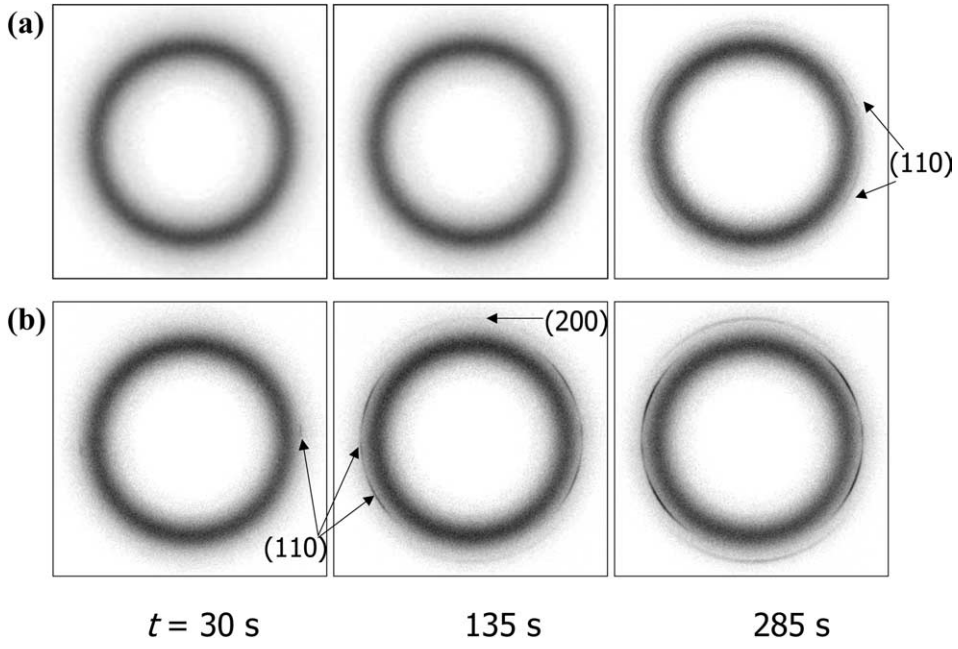

Fig. 27. Selected 2D WAXD patterns of (a) MB-100k/MB-250k (95/5) and (b) MB-100k/MB-250k (90/10) after shear cessation. [Reprinted with permission from Macromolecules 2004;37(13):4845. Copyright (2004) American Chemical Society].

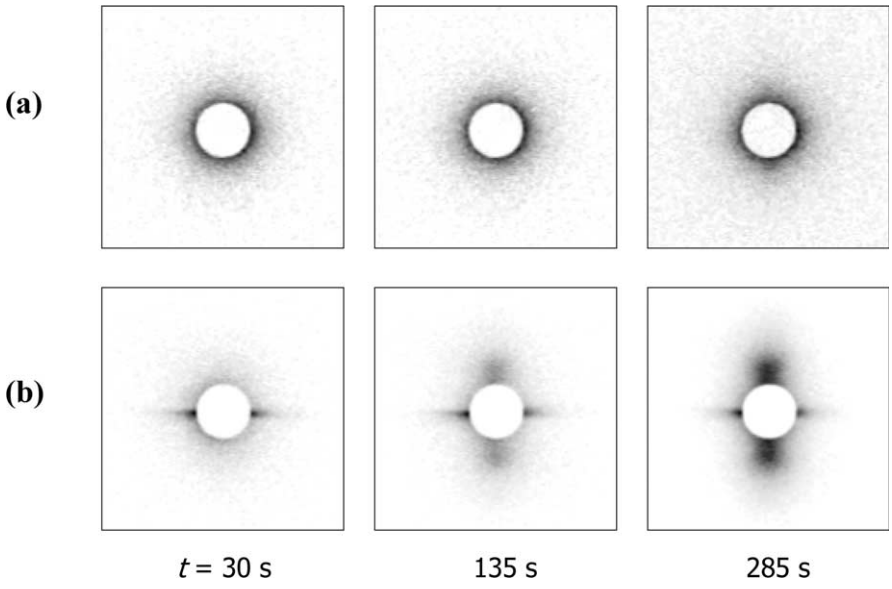

Fig. 28. Selected 2D SAXS patterns of (a) MB-100k/MB-250k (95/5) and (b) MB-100k/MB-250k (90/10) after shear cessation. [Reprinted with permission from Macromolecules 2004;37(13):4845. Copyright (2004) American Chemical Society].

or kebabs in the melt. On the other hand, SAXS patterns of the MB-100k/MB-250k (90/10) blend were remarkably different from the above observations. The pattern immediately after shear (at $t=30$ s) exhibited an equatorial streak with no indication of meridional maxima. The meridional maxima only emerged at a later time, which could be clearly identified in the pattern at $t=135$ s. Subsequently, as crystallization progressed, the equatorial and meridional scattered intensities increased with time, as seen in Fig. 28(b).

The following conclusions were drawn from the above results. First, it was shown that shish formed first followed by kebabs, which was evident from the emergence of the equatorial streak immediately after shear followed by the meridional maxima. Second, the sharp, spot-like, equatorial reflection in the WAXD pattern of Fig. 28(b) can be attributed to the shish structure that consist of extended chain crystals oriented parallel to the flow direction. Thus, in the MB-100k/MB-250k (90/10) blend under shear, formation of shish structure with a length on the order of 1000 Å and a diameter on the order of 100 Å (details in an earlier publication) was evident from the initial development of the equatorial streak in SAXS and the simultaneous appearance of two equatorial (110) reflections in WAXD. The immediate formation of a relatively large shish structure in the MB-100k/MB-250k (90/10) blend indicated that the crystallization process started in highly oriented MB-250k chains. Note that in spite of the lack of a direct evidence of the shish formation in the blends containing lower amounts of high molecular weight components, the final shish-kebab morphology observed in these systems is a clear indicator of the existence of oriented chains or shish precursors. The earlier results of iPP studies also support the above scenario. Therefore, we concluded that the formation of initial shish and the subsequently formed kebab crystals must originate from the oriented segments of chains induced by flow.

3.1.4.2. Crystallization kinetics of the shish-kebab structure from MB-250k PE. Time evolution of the total crystallinity for the two-blend series: MB-50k/MB-250k (100/0, 97/3, 95/5 and 90/10) and MB-100k/MB-250k (100/0, 93/7, 95/5, 90/10) is shown in Fig. 29(a) and (b), respectively. In Fig. 29(a), all MB-50k/MB-250k blends showed a relatively fast crystallization behavior immediately after shear. The final values of the total crystallinity at the end of the measurements were approximately 2.8, 4.8 and 6.2% for 97/3, 95/5 and 90/10 blends, respectively. The 3 wt% blend exhibited the slowest crystallization kinetics among the chosen three compositions. A similar behavior was also seen in MB-100k/MB-250k blends (Fig. 29(b)). The final values of the total crystallinity in the MB-100k/MB-250k blends were approximately 2.3, 4.7 and 5.3% for 97/3, 95/5 and 90/10 blends, respectively. Compared to MB-50k/MB-250k blends, the MB-100k/MB-250k blends showed notably slower kinetics at the same experimental conditions. It was seen that the total crystallinity level was always lower than the weight percentage of the MB-250k linear polymer; and the crystallinity of the two low molecular weight matrices (MB-50k and MB-100k) was zero during the experimental time period ($\sim$45 min). These observations indicated that in the blends the crystallization behavior resulted mainly from the transition in the MB-250k component, which was dispersed in an amorphous polymer matrix of low M_w. Thus, the blends exhibited a 'dilute solution'-like condition. Interestingly, the different crystallization kinetics of the two series of the blends, MB-50k/MB-250k and MB-100k/MB-250k (at shear rate $=60\ s^{-1}$, shear time $=5$ s, $T=$

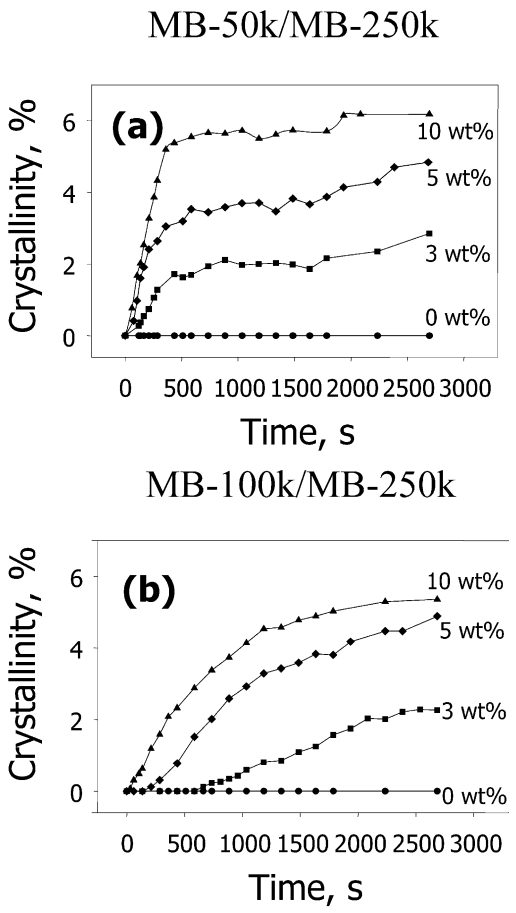

Fig. 29. Evolution of the total crystallinity in (a) MB-50k/MB-250k (100/0, 93/7, 95/5 and 90/10), and (b) MB-100k/MB-250k (100/0, 93/7, 95/5 and 90/10) blends after shear as a function of time. [Reprinted with permission from Macromolecules 2004;37(13):4845. Copyright (2004) American Chemical Society].

120 °C), were shown to be due to the matrix viscosity, which affected the translation or diffusion of high molecular weight chains.

In the second study, inspired by the above results, the same MB-50k polymer was used as the matrix component, and 2 wt% of an ultra-high molecular weight polyethylene (UHMWPE) sample, having M_w of $5–6\times10^6$ g/mol and a MWD of about nine, was used as the minor crystallizing component. The results revealed the observation of an unexpected shish-kebab structure with multiple shish, which will be described later.

3.1.4.3. MB-50k and UHMWPE blend. In these experiments, the experimental temperature was 128 °C (i.e. 8 °C higher than the temperature in the MB-250k study), where the MB-50k matrix remained completely non-crystalline and, thus, allowed investigation of only the crystallization behavior of UHMWPE under flow. Fig. 30 shows selected 2D SAXS and WAXD patterns of the MB-50k/UHMWPE blend at different times after cessation of shear (shear rate = 60 s^{-1}, shear time = 5 s, T = 128 °C). The initial SAXS pattern (t = 30 s) exhibited an equatorial streak, due to shish, with no indication of meridional maxima. The meridional maxima, due to kebabs, appeared only at a later time. By the end of the experiment (t = 2610 s), a very clear shish-kebab morphology developed in the polymer melt, where the only crystallizing species was the UHMWPE.

The WAXD pattern at t = 30 s showed a pair of sharp (110) reflections on the equator, which confirmed that shish was constituted of the extended chain PE crystals. The subsequent crystallization led to the superposition of (110) and (200) arc-like equatorial reflections on the initial line-like (110) reflection with increased intensity and slightly decreased orientation degree (see t = 135 s and 2610 s in Fig. 30). In addition, the appearance of (200) reflections on the equator indicated that the lamellar stacks of UHMWPE (or kebabs) were flat instead of twisting [1].

Fig. 31 shows the time evolution of the total crystallinity (WAXD) for MB-50k/UHMWPE at 128 °C after cessation of shear. The total crystallinity at the end of the experiment was around 2%, which was about the same as the UHMWPE concentration. This finding suggested that the shish-kebab structure mainly resulted from the crystallization of UHMWPE. In other words, only the UHMWPE chains participated in the formation of the shish-kebab structure, while the low molecular weight matrix chains acted as the 'solvent' molecules and were not involved in crystallization. The contributions of shish and kebab crystals to the total crystallinity, estimated from the SAXS results, are also shown in Fig. 31. It was seen that the crystallinity of the shish ($X_{c,shish}$) increased rapidly and reached a plateau level ($X_{c,shish} \approx 0.08\%$ at t = 30 s, $X_{c,shish} \approx 0.15\%$ at $t > 75$ s), while the crystallinity of the kebabs dominated the total crystallinity growth ($X_{c,kebab} \approx 1.85\%$ at t = 2610 s). Time evolution of long period (L) between the adjacent kebab layers (lamellae), as determined by the position of the meridional scattering maximum in SAXS (Fig. 30), is shown in Fig. 32. The L value was found to remain at around 40 nm throughout the entire crystallization process, except in the beginning of the crystallization stage where a slight decrease (from 42 to 40 nm) was seen.

The above results can be explained by the concept of coil–stretch transition in polymer melts. Recall that the coil–stretch transition has two-fold criticality: For a given M there is a critical strain rate and for a given strain rate there is a critical M (Fig. 2). The studies of MB-50k/MB-250k and MB-100k/MB-250k blends showed that MB-250k molecules stretched and formed shish structures at the imposed shear condition: Rate = 60 s^{-1}, duration = 5 s. We can conclude that the critical M (M^*) value of PE under these shear conditions should be less than or about the same order as 250,000 g/mol. Hence, almost all of the UHMWPE chains are above the M^* threshold and can undergo the coil–stretch transition under identical shear condition. In such a case, one would expect the formation of a substantial fraction of shish crystals in the sheared melt. However, the shish fraction in the shish-kebab structure was relatively

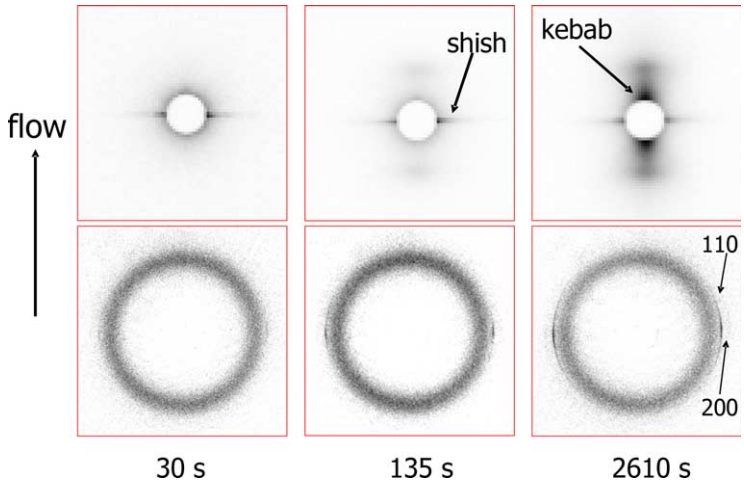

Fig. 30. 2D SAXS and WAXD patterns of MB-50k/UHMWPE (98/2) after cessation of shear (shear rate = 60 s^{-1}, shear time = 5 s, T = 128 °C).

small (only 8%), even at the end of the experiment, Fig. 31. An alternate scenario is that probably only certain segments of the UHMWPE chains underwent the coil–stretch transition, not the entire chain. The stretched segments in UHMWPE were responsible for the shish formation, while the coiled segments formed the kebabs. It is rather unlikely that the ensemble of the oriented UHMWPE chains in flow resulted in a mixture of fully extended and coiled chains.

To support the above interpretations, a study involving direct, visual observation of the finer details of UHMWPE shish-kebab structures by ex situ electron microscopy was undertaken [76]. The following characteristics of UHMWPE shish-kebabs were determined from the electron micrographs: Length and diameter of the shish and their distributions, lateral size of kebabs, and the distribution of kebabs grown on the shish. The results are presented below.

3.2. UHMWPE shish-kebabs with multiple shish by ex situ electron microscopy

For a clear view of the shish-kebab structure generated under flow, it is absolutely essential to extract the shish-kebab moieties from the surrounding matrix containing crystalline (spherulites) and amorphous polymers that overwhelm its finer details in the sheared blends. To achieve this, the recovered sheared sample at the position of the X-ray illumination was subsequently treated with hot toluene at 100–105 °C. Under this condition, the low molecular weight PE copolymer matrix (MB-50k) was dissolved in hot toluene, while UHMWPE crystallites were maintained. The hot MB-50k/toluene solution with insoluble UHMWPE residues was filtered with a 0.5 μm PTFE filter at 100 °C. The UHMWPE residues were further washed by fresh toluene at room temperature twice, and were dried in a vacuum oven for 24 h. The dried sample was directly examined by Zeiss DSM 982 Gemini field-emission scanning electron microscopy (FE-SEM) at an accelerating voltage of 2.0 kV. No or very slight heavy metal coating was applied to preserve the sample morphology at high magnifications. Part of the samples was also etched by fuming nitric acid at 60 °C for 24 h (the suitable time period was determined after several trials) [117]. The etched

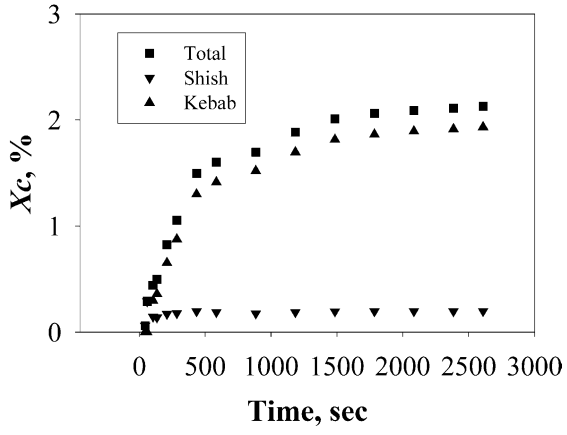

Fig. 31. Time evolution of the total crystallinity (X_c), crystalline fractions of shish and kebabs for MB-50k/UHMWPE (98/2).

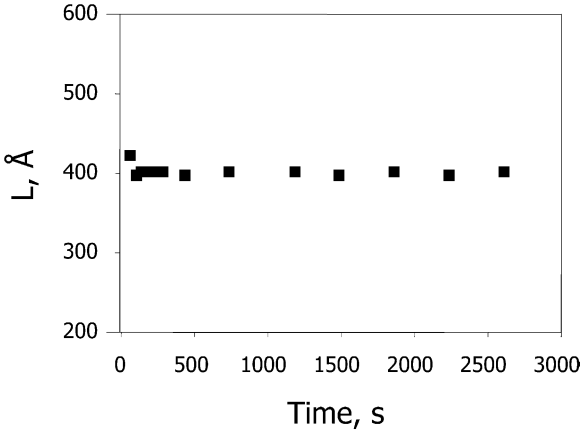

Fig. 32. The average long period change during the kebab development as a function of time.

samples were washed by double-distilled water and acetone repeatedly a couple of times and were dried in a vacuum oven before the SEM study.

Fig. 33 shows four representative FE-SEM micrographs taken at different magnification and/or sample locations. All showed that shish-kebab morphology formed in the sheared MB-50k/UHMWPE blend, as expected. As shown in Fig. 33(a), the average diameter of the outer kebabs is approximately 300–400 nm. The total shish-kebab entity is considerably long, certainly on the order of μm (some even longer than 10 μm). The micrographs indicated a wide distribution in the overall shish length. It is known that the average radius of gyration of the UHMWPE chains in the melt is around 110 nm [117] and the average extended chain length is about 25 μm. The micron size shish-kebab entities clearly point towards the presence of highly extended chains in the sheared melt prior to crystallization.

A closer, magnified view revealed the finer structure of shish-kebabs, (Fig. 33(b)–(d)). The most striking feature in these images is that the adjacent kebabs are seen to be interconnected by several short length shish aligned parallel to each other, instead of a single central core. The micrographs clearly show that these short shish sections are not necessarily connected with each other. The average diameter of these shish is about 10 to a few tens of nanometers. The average distance between the neighboring kebabs is 30–60 nm, consistent with the calculated values of the long period ($\sim$40 nm, Fig. 32) from in situ SAXS data. This shish structure is quite different from the conventional view, where only one shish is thought to be present [101, 102,104,105]. We termed the observed structures, connecting adjacent kebabs, as 'multiple shish'. These seem to arise from fully extended chain sections between the kebabs or probably junctions of entangled chain networks. One possibility is that chain segments that are away from the entanglement points can experience the highest degree of orientation due to imposed flow. If we apply the de Gennes theory [22] of the chain conformation dynamics in flow to the chain length between entanglement points, these segments could undergo a coil–stretch transition resulting in fully extended chain sections. The substantially longer length of the shish-kebab entity observed in SEM suggests that the linear connectivity of many chains may be maintained through the network junctions, which could be incorporated as a defect in the shish structure. We speculate that these multiple shish could link together either by themselves or by the growth of kebabs at a later stage of crystallization.

The micrographs in Fig. 33(d) also revealed other features of the shish-kebab structure, a few unexpected and rather peculiar. (1) The shape of the kebabs clearly resembles that of folded-chain PE lamellar crystals with distinct facets. (2) The growth of adjacent kebabs follows a preferred orientation, almost 90° to the shish-axis, rather

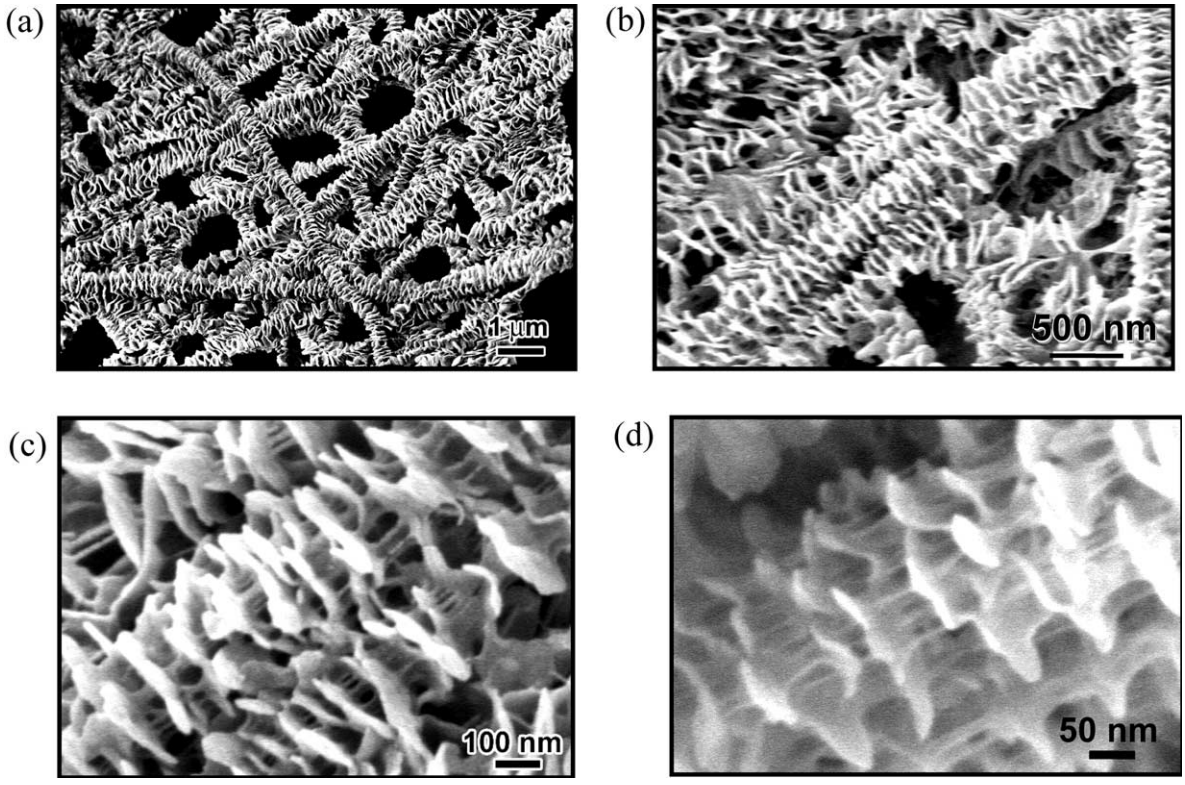

Fig. 33. Micrographs of UHMWPE shish-kebabs by field-emission scanning electron microscopy (FE-SEM). Multiple shish can be clearly seen between adjacent kebabs in high resolution images (e.g. (d)). (Reprinted with permission from Phys. Rev. Lett. 2005;94(11):117802. Copyright (2005) American Physical Society).

than an irregular or random pattern. (3) The average size of the kebabs is about the same. Although observation (2) is expected, the precision of angular orientation of the kebabs was not an a-priori thought or expected. Similarly, the high degree of uniformity in the size of kebabs was also unexpected. It is a strong evidence of the instantaneous or athermal nucleation condition for the primary nuclei. We do not know if the above features are due to the particularity of the sheared-induced UHMWPE shish-kebab structure, or a general phenomenon in all flow-induced shish-kebab structures in entangled polymer melts. This will be a subject of our future study.

In the next step of the electron microscopy studies, the fuming nitric acid etching treatment was applied to the extracted shish-kebab moieties. We hope that with this treatment the less stable folded-chain kebab crystals can be etched away from the surface of the central shish core, leaving the more stable extended chain shish crystals for further observation. Fig. 34 shows an SEM micrograph of the recovered shish core. The average shish length is longer than 500 nm, most probably in the μm range. The shish diameter ranges from 10 to 50 nm, consistent with the earlier observations in solvent extracted samples. Interestingly, the overall structure appears to be network-like, i.e. the shish are seen to be interconnected. The above picture of the shish core points towards the following scenarios. First, the successful extraction of the kebab overgrowth leaving behind a long shish core leaves no doubt that the shish form first, later followed by kebabs, as observed by in situ X-ray observations. Second, the micron-long shish indicated a large value of the mean chain extension of chains in the shish; consistent with the UHMWPE chains. Third, the network-like appearance of the shish core structure meant that the entanglement junctions existed at the time of shish formation. These observations support the conclusion that in entangled polymer melts, the coil–stretch transition occurs between the entanglement junctions. In addition, the above observations indicated that shish consist primarily of high molecular weight chains, because only long chains can maintain the linear connectivity through the entanglement points, which is required for the observed micron long shish.

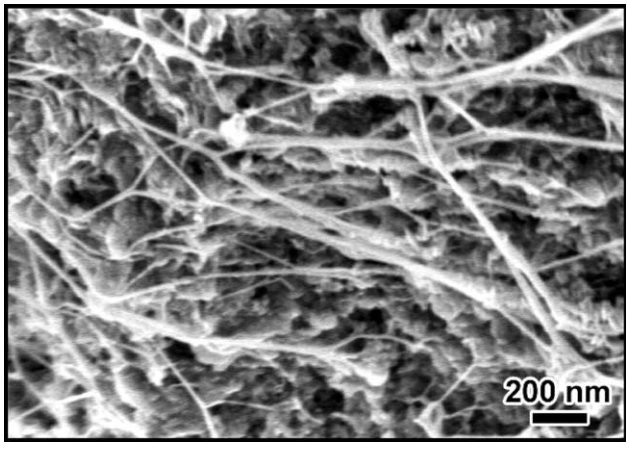

Fig. 34. SEM micrograph of UHMWPE shish after dissolution of the kebab overgrowth.

It should be noted that some researchers may not identify with the above presented concepts of multiple shish, as pointed out by one of the reviewers. For example, the observed structures can be viewed as filaments tying kebabs together that have an appearance similar to craze interiors and to intercrystalline links observed by Keith et al. [118] in the electron micrograph of high molecular weight polyethylene, crystallized from a blend with low molecular weight paraffin from which the paraffin had been chemically removed. The fibrillar links were seen to bridge radial arms of the spherulites and each link appeared to be like an extended chain crystal. These structures indeed appear similar to those of multiple shish and kebabs described above. However, the origin of the two is not likely to be the same. In the case of quiescently crystallized melts, as in the system studied by Keith et al. [118], the authors envisioned the following. During crystallization process a chain may occasionally come into contact with surfaces of different and widely separated crystals, and begin to crystallize. Subsequently, the molecules continue to crystallize until they are pulled taut, forming the ties or bridges that provide the nuclei for crystallization of other molecules. In this case, the lamellae form first and the bridges of extended chain crystals of high molecular weight tie chains form later. In the case of shear-induced shish-kebab structures, the results of rheo-X-ray experiments are unequivocal that shish evolve first followed by decoration of regularly placed kebabs. The remarkable uniformity in the size and diameter of kebabs indicates the uniformity in the time of their inception (or nucleation), and the pre-existence of long, extended chain structures (or shish). Furthermore, the multiple links observed in the electron micrographs point towards the formation of aligned group/bundle of extended chain sections. The long shish indicate linear connectivity of the links or the participating chains maintain the orientation/extension through the entanglement points.

We emphasize that the above results are the first of their kind and certainly warrant further studies to elucidate the exact mechanism of the multiple shish formation as well as to explore if the observation is a universal phenomenon in entangled polymer melts. Our thoughts on a model of the molecular mechanism of shish-kebab formation are presented later.

3.3. In situ rheo-optical studies of iPP

Various in situ rheo-optical techniques [61–70,119,120] have been used to investigate flow-induced crystallization. Some very interesting results were obtained in the early stages of crystallization. For example, Winter et al. [61–63] detected, by simultaneous small-angle light scattering (SALS) technique, density fluctuations prior to the

appearance of crystalline structures during crystallization of iPP under oscillatory shear. Kornfield et al. [58,70] observed an unexpected upturn in birefringence in iPP polymer melt at a high temperature of 175 °C (above the nominal melt point) after shear. The relationships between the optical results and the structural information at the molecular and nanoscopic levels are not yet well developed, probably because the wavelength (of several hundred nanometers) is too large to directly probe the structure.

In this section, we present results from a rheo-optical study of the same iPP polymer, as described in Section 3.1.1. This study was carried out jointly by the Winter group and our group [52]. The optical micrographs of the shear-induced oriented structures provided the complementary information on the structural changes in shear at the micrometer scale. In situ rheo-optical experiments were performed using a Universal Polarizing Microscope (Carl Zeiss, Inc., model ZPU01) equipped with Linkam shear stage (CSS 450, similar to the one used in the above shear-X-ray experiments). The conditions for the rheo-optical experiment were as follows: Shear rate $= 10\ s^{-1}$, $t_s = 60$ s, $T = 148$ °C. Optical micrographs were taken during crystallization of iPP melt at selected intervals after cessation of shear.

A series of polarized optical micrographs at selected times after shear are shown in Fig. 35. These pictures showed that micron size fibrillar (thread-like) structures were formed immediately after shear. The unoriented spherulitic structures were seen to emerge at the later stages (e.g. $t = 300$, 900 s). The first image was taken near the instant of flow cessation ($t = 60$ s), which clearly showed that birefringent fibrils had already formed, as seen on the dark field of residual amorphous melt. The fibrils are oriented parallel to the flow direction. Subsequently, they grew in thickness, as evidenced from the later micrographs ($t = 180$–1200 s). The micrographs after several hours ($t =$ 8100 and 43,200 s) showed that spherulites cover the whole field and overwhelmed the fibrillar morphology; the fibrils were no more visible in the microscope. The sample was left in the microscope and then was heated again. Upon heating, the spherulitic structure disappeared (melted) at about 165 °C and fibrils became visible again in the microscope. The fibrillar morphology was apparent until about 175 °C, at this temperature the fibrils disappeared (melted). This is direct, visual evidence that the shear-induced oriented microscopic fibrillar morphology is preserved, stable and possesses a higher melting point than the unoriented spherulites.

It should be noted that optical micrographs showed morphological features on a larger length scale than the earlier SAXS and WAXD results. The features of shear-induced fibrils became visible when the diameter was above 1 μm and higher. The large diameter of these fibrils indicated that each fibril should contain many shish-kebab assemblies. The fibrillar structures observed in the initial stages by optical microscopy were consistent with the morphology of macroscale cylindrites [16–18,121–123].

4. Modeling of SAXS data based on shish-kebab structure

It is clear that the development of shish-kebab structure can be directly observed by the rheo-SAXS technique (Section 3.1). However, the observed scattering images are in the reciprocal space, which need to be analyzed with a suitable model. In collaboration with Burger, we have developed a model in closed analytical form for small-angle scattering of a shish-kebab structure [124]. This model can be used to analyze the SAXS data and obtain the relevant information about the kebab morphology, but not shish.

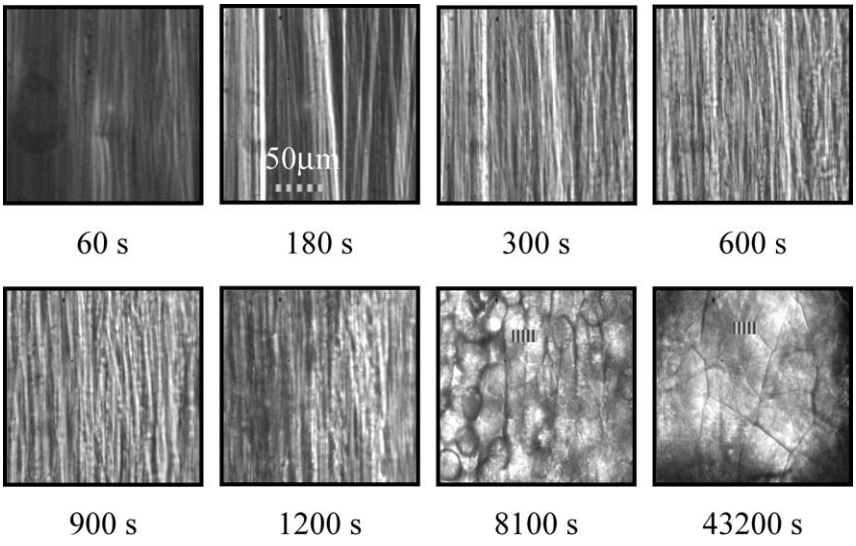

Fig. 35. Optical micrographs taken at selected times during shear-induced crystallization of iPP (rate $= 10\ s^{-1}$, $t_s = 60$ s, $T = 148$ °C). [Reprinted with permission from Macromol Symp 2002;185:105. Copyright (2002) Wiley-VCH Verlag GmbH and Co. KGaA, Weinheim].

This limitation does not hamper the usefulness of the approach because, in many cases, the presence of shish cannot be detected by SAXS due to the non-crystalline nature or low concentration.

4.1. Closed analytical form of shish-kebab model

The model consists of a central shish and a periodic arrangement of disk-like kebabs as shown in Fig. 36. The spatial arrangement of the shish-kebabs is assumed to be uncorrelated so that the predictions are based on a single shish-kebab structure. The shish-kebab model is assumed to have a cylindrical symmetry around the shish-axis. The kebabs are represented as disks with a diameter distribution $h_D(D)$ and a thickness distribution $h_T(T)$, which are assumed to be statistically independent. The distance distribution between the centers of the nearest neighboring disks is given by a long period distribution $h_L(L)$, again assumed to be statistically independent of next neighbor distances and also of the disk size parameters. The moderately ordered stack of disks is further assumed to have an infinite height. Although a finite stack height can be easily added here, for the parameters and scattering vector range of interest, its effect will be indistinguishable from stacking disorder. In this model, the scattering due to kebabs, i.e. along the meridian, is of primary concern, whereby the scattering contribution of the shish is neglected.

Using a standard substitution disorder approach, with the absolute value of the scattering vector $s = |\vec{s}| = 2\lambda^{-1}\sin\theta$ (where λ is wavelength of the X-ray beam and θ is half of the scattering angle), $\vec{s} = (s_1, s_2, s_3)$ and $s_{12} = (s_1^2 + s_2^2)^{1/2}$ (the subscript 3 represents the direction along the shish axis), the scattering intensity $I(s_{12}, s_3)$ of the shish-kebab structure can be expressed as follows:

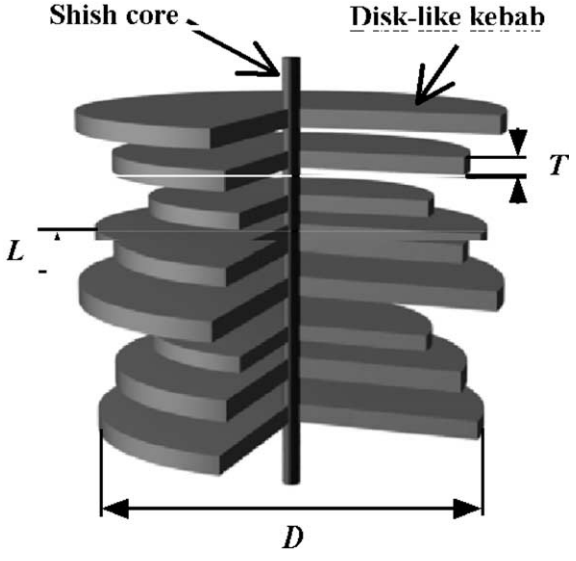

Fig. 36. The shish-kebab model for 2D SAXS calculations. Kebab diameter D, thickness T are arranged in a moderately periodic fashion with distances L. A sector has been cut out to enhance visibility.

$$I(s_{12}, s_3) \sim K_s[\langle|A(s_{12}, s_3)|^2\rangle_{D,T} - |\langle A(s_{12}, s_3)\rangle_{D,T}|^2 + |\langle A(s_{12}, s_3)\rangle_{D,T}|^2 |Z_L(s_3)|^2] \quad (3)$$

In this equation, the scaling parameter, K_s, includes (1) a constant prefactor due to the electron density difference, $(\Delta\rho)^2 = (\rho_c - \rho_a)^2$, between crystalline ($\rho_c$) and amorphous phases ($\rho_a$), (2) a factor $\phi(1-\phi)$, where ϕ is the crystalline volume fraction, and (3) a factor, $H_z^2 = \exp(-2\pi d_z^2 s^2)$, due to the finite density transition at the interface, and other approximation constants that are not known in the calibration of absolute scattered intensity.

In Eq. (3), $A(s_{12}, s_3)$ is the form factor describing the Fourier transform of the density distribution of a single disk (lamellae) of diameter, D, and thickness, T.

$$A(s_{12}, s_3) = \frac{\pi D^2}{4}\frac{2J_1(\pi D s_{12})}{\pi D s_{12}} T \frac{\sin(\pi T s_3)}{\pi T s_3} \equiv \frac{\pi D^2}{4} A_2(D s_{12}) T A_1(T s_3) \quad (4)$$

where we have introduced the abbreviated notation A_1 and A_2, in which the index can be considered as a dimension (A_1 and A_2 are one- and two-dimensional, respectively). Because h_D and h_T are assumed to be statistically independent, their averages can be factorized:

$$|\langle A(s_{12}, s_3)\rangle_{D,T}| = \langle\frac{\pi D^2}{4} A_2(D s_{12})\rangle_D \langle T A_1(T s_3)\rangle_T \quad (5)$$

$$\langle|A(s_{12}, s_3)|^2\rangle_{D,T} = \langle\frac{\pi^2 D^4}{16} A_2^2(D s_{12})\rangle_D \langle T^2 A_1^2(T s_3)\rangle_T \quad (6)$$

When the diameter (D) and thickness (T) are completely monodisperse, the first two terms in Eq. (3) would cancel each other, leading to the familiar product of form factor and lattice factor.

The lattice factor $|Z_L(s_3)|^2$ is given by [125],

$$|Z_L(s_3)|^2 = \mathrm{Re}\left(\frac{1 + H_L(s_3)}{1 - H_L(s_3)}\right) \quad (7)$$

where $H_L(s_3)$ is the one-dimensional Fourier-transform of $h_L(L)$. The traditional choice for $h(L)$ would be a shifted Gaussian [126,127],

$$h_L(L) = (2\pi\sigma_L^2)^{-1/2}\exp\left[-\frac{(L - \bar{L})^2}{2\sigma_L^2}\right] \quad (8)$$

However, if the stacking periodicity is highly disordered (i.e. σ_L is large) there will be an unreasonable tail of the distribution at negative values. Therefore, we chose the following Γ-distribution, which does not suffer from this problem [128].

$$h_L(L) = \frac{1}{\Gamma(\nu_L) L_O}\left(\frac{L}{L_O}\right)^{\nu_L - 1}\exp\left(-\frac{L}{L_O}\right) \quad (9)$$

$$H_L(s_3) = (1 - 2\pi i L_O s_3)^{-\nu_L} \quad (10)$$

where the parameters L_O and ν_L depend on the average value (center), $\bar{L}$, and standard deviation, σ_L, thus they can be read as $L_O = \sigma_L^2/\bar{L}$ and $\nu_L = \bar{L}^2/\sigma_L^2$.

A bell-shaped density distribution, which works well for both h_D and h_T, and for which the required averages can be calculated analytically, is given by ($X = D$ or T, respectively):

$$h_X(X) = \frac{2}{\Gamma(\nu_X)}\left(\frac{X}{X_O}\right)^{2\nu_X-1}\exp\left[-\left(\frac{X}{X_O}\right)^2\right] \tag{11}$$

Eq. (3) together with (4)–(7) (the parameters X_O and ν_X need to be evaluated by numerical iteration) provide a complete analytical solution for the SAXS of shish-kebab structure. We are now in a position to explore how the SAXS depends on the various parameters.

4.2. Simulation of 2D SAXS pattern from shish-kebab model

The most important difference between a shish-kebab structure and a traditional lamellar stack is the average lateral lamellar size (D) and polydispersity (σ_D). A traditional lamellar stack, like the one inside a spherulite, is a compact object with a fairly uniform lateral size, which can often be assumed to be infinitely large on the length scale of interest. For a shish-kebab structure, the average lateral lamellar size is much smaller (in the range of tens of nanometers) and non-uniform, which leads to a relatively large σ_D.

Generally speaking, the physical implication of the lateral lamellar size polydispersity, σ_D, is as follows. If the value of σ_D is small, which suggests that all lamellae have a similar lateral size distribution (or they are nucleated at about the same time), then the nucleation condition may be instantaneous (i.e. athermal nucleation). If the value of σ_D is large, which suggests that the lamellae have a large distribution of the lateral size (or they are nucleated at different times), then the nucleation may be sporadic (thermal nucleation). The value of σ_D has a profound effect on resulting scattering features, such as the scattering intensity at low angles and the distinction of the interference maxima (scattering peak). Calculated 2D SAXS patterns using the shish-kebab model (Eq. (8)) at two different σ_D values ($\sigma_D = 10$ and $\sigma_D = 50$) are shown in Fig. 37. It is seen that at a lower σ_D value ($\sigma_D = 10$), two distinct scattering maxima are seen along the meridional direction; whereas at a higher σ_D value ($\sigma_D = 50$), since the point reflection becomes broader and weaker, the intensity at low angles relatively increases and the interference maximum becomes diffuse. The scattering pattern calculated from the $\sigma_D = 10$ conditions resembles the typical SAXS pattern observed from well oriented semi-crystalline polymers with uniform lamella diameters; while the scattering pattern calculated from the $\sigma_D = 50$ conditions resembles the 'meridional streak' pattern observed at the initial stages of crystallization under shear. In other words, the two-point SAXS pattern would indicate a small variation in the lateral kebab size (i.e. a small σ_D), while the meridional streak SAXS pattern would indicate a large variation in the lateral kebab size (i.e. a large σ_D).

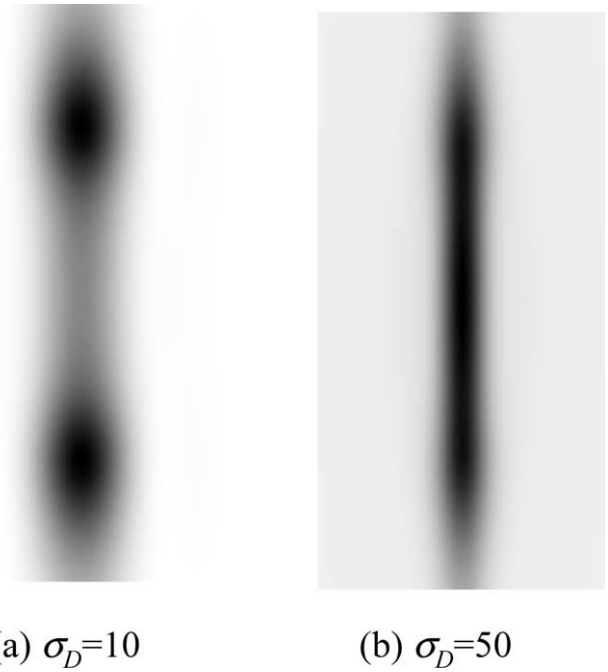

Fig. 37. Calculated 2D scattering pattern based on $I(s_{12},s_3)$, for $L = 40$ nm, $\sigma_L = 15$, $T = 15$ nm, $\sigma_T = 5$, $D = 100$ nm, and σ_D as indicated. The displayed range extends to $s_{12} = 0.02\ \text{nm}^{-1}$ and $s_3 = 0.04\ \text{nm}^{-1}$. Both images have been scaled for maximum contrast. A low lateral lamella size polydispersity leads to a two-point pattern whereas increasing the lateral lamella size leads to increased scattering at small angles.

An increase in the polydispersity of the lamellar thickness (σ_T) would also increase the overall density fluctuations, resulting in the production of strong scattering at small angles. However, we believe that the σ_T value would not be too large at the initial stages of crystallization under isothermal conditions; this is because the lamellar thickness is a thermodynamic variable that should vary only with temperature. The variation of the lamellar stacking disorder (or the polydispersity of lamellar long period), σ_L, also affects the scattering profile, similar to the effects of polydispersities in lamellar diameter and in thickness. It is interesting to note that, under the combined condition of large σ_L and large σ_T values (i.e. both polydispersities of the lamellar long period and the lamellar lateral size are large), the scattering maximum can disappear completely. The physical implication of the σ_L value may be related to the type of the nucleation. Under sporadic nucleation condition, the value of σ_L is expected to be large; whereas under instantaneous nucleation condition, the value of σ_L is expected to be small.

The treatment so far only considered the perfectly oriented case. Although, it is straightforward to introduce finite preferred orientation into our model, the required integrations can no longer be performed analytically. Also,

it will be difficult to distinguish the effect of finite preferred orientation from the mean lateral stack size. The ambiguity could only be resolved if significant scattering would be available at higher angles, e.g. a second order interference maximum.

4.3. Experimental fitting using shish-kebab model

The major advantage of the above analytical model is that it provides a relatively easy tool for fitting of experimental SAXS data, which allows one to extract useful structural information during the development of shish-kebabs. The parameters, D, T, L and their distributions, can be estimated by fitting of a 2D SAXS intensity pattern or series of 1D SAXS profiles using the shish-kebab model. The typical fitting results are as follows. Fig. 38 shows the meridional SAXS profiles of a binary PE blend at different crystallization time, t, after shear and the corresponding fits using the 6-parameter (L, T, D, σ_L, σ_T, and σ_D) shish-kebab model. In Fig. 38, at short crystallization times (e.g. at 60 s), the scattering profiles exhibit a faint but discernable first-order interference maximum; at long crystallization times (e.g. at 435 s), the profiles exhibit strong scattering at the low s region, whereby the interference maximum peak becomes diffuse. At very long crystallization times (e.g. >2535 s), the meridional scattering profile becomes almost completely diffuse, unlike the typical pattern observed from oriented semicrystalline polymers. This suggests that the lamellar (kebab) stack is highly oriented with the axis pointing into the flow direction but probably having broad distributions in both kebab diameters as well as long spacing in the shish-kebab structure.

From the extracted parameters, perhaps the most interesting result is the time-evolution of the kebab size. It was found that the kebab size (D) increased with time (t), but not in a linear fashion. In other words, the kebab growth rate ($G(t)=\mathrm{d}D/\mathrm{d}t$) is not constant. For a series of MB-50k/UHMWPE blends having different UHMWPE concentrations, the plot of $G(t)$ rate versus time is shown in Fig. 39, which exhibited the diffusion-controlled process (i.e. $G(t)\propto t^{-1/2}$). Typically, the secondary nucleation theory of polymer crystallization in quiescent state predicts a constant spherulitic growth rate, where the mass diffusion is not the limiting barrier. However, the recent AFM study of crystallization at nanometer scale by Hobbs et al. [35] contradicts the above; growth was found to be sporadic in time and space. He envisioned a stronger role for diffusion process. In addition, the simulation work of the early stage shish-kebab formation in elongational flow by Muthukumar et al. [28] clearly showed that the kebab growth was significantly influenced by the rate of addition or diffusion of chains. Thus, the diffusion-controlled kebab growth in the PE blend is, although not totally unexpected, another significant finding of the present study. It is our opinion that, in flow and especially at the early stages of crystallization, the dynamics of chain motion/relaxation of chains near the kebab growth front can affect the kebab growth rate, and hence the observed deviation from the conventional view. Further studies of this rather unusual observation are in progress.

5. Molecular mechanism for shish-kebab formation

In this section, we discuss the molecular origin of the shish-kebab formation, based on the above experimental results. Recall that the most striking findings of the above studies are two, both related to the formation of shish. (1) Flow-induced precursor structures, which may contain amorphous, mesomorphic and/or crystalline phases, provide a scaffold of primary nuclei in the sheared polymer melt for

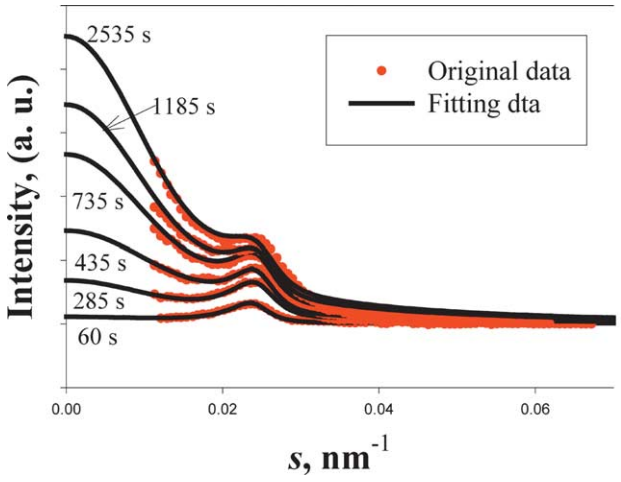

Fig. 38. Estimation of D, T, L and their distributions by fitting of the SAXS data of a model PE blend under shear.

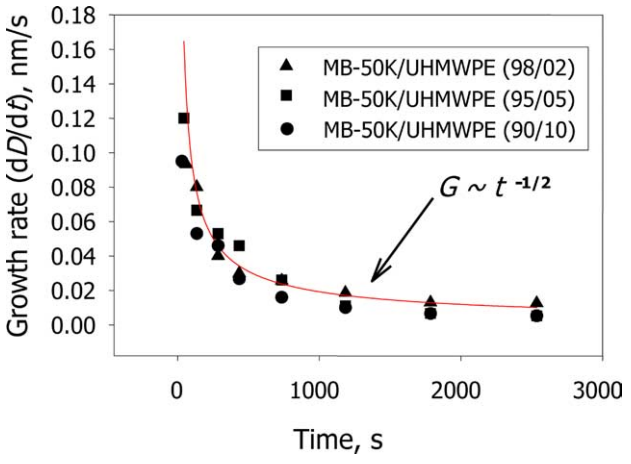

Fig. 39. The calculated kebab growth rate ($G(t)=\mathrm{d}D/\mathrm{d}t$) curve for the model PE blends. Results indicate that the kebab growth follows a diffusion-control process, i.e. $G(t)\sim t^{-1/2}$.

further crystallization. This is seen from in situ X-ray studies of several polymers and blends (iPP, PE, iPP/aPP, PE/UHMWPE). (2) The formation of multiple-shish between the kebabs that is evident by SEM observation in solvent extracted sheared sample. These results indicate a molecular mechanism, different from the 'conventional' view, for the formation of shish in an entangled melt. In the following, we present our interpretations for the origin of shish in the sheared melts with a particular emphasis and the subsequent formation of kebabs.

5.1. 'Conventional' view of shish formation

As mentioned above, the flow-induced shish-kebab morphology in an entangled melt is no different, on a macro-scale, than that in dilute or concentrated solutions, even when the imposed flow conditions are different; i.e. elongational, shear or mixed. The differences arise on a micro-scale, and especially in the sheared entangled melts because of (a) the tumbling effect of the rotational component, and (b) the presence of entanglements.

The shish formation can be related to the single chain dynamics under flow. The recent experimental results of dilute polymer solution studies by Chu et al. [31] showed that the chains exhibit distinct conformational shapes with differing dynamics in elongational flow. It should be noted that this is true specifically for transient chain conformations and not the final steady-state conformation, which indeed exhibit fully stretched states in accordance with the predictions of coil–stretch transition. It was found that the rate of stretching of individual chains was highly variable and depended on the initial, random coil conformation. Their studies in shear flow [32] showed that, in steady-state shear, the mean fractional extension, $\langle x/L \rangle$, increased gradually with imposed flow strength. The effects of extensional and rotational components of a shear flow are schematically presented in Fig. 40. The extensional components orient and/or stretch polymer molecules, the rotational components cause end-over-end tumbling and the stretched state is destabilized. Thus, molecules stretch, tumble, and retract in a stochastic manner. Since, both the stretching and tumbling are driven by the velocity gradient, the random stretching and contraction process occurs more frequently at higher shear rates; hence the mean extension reaches a plateau value, below the full contour length, even in very strong shear flows (Fig. 15).

In concentrated solutions or entangled melts in elongational flow, Keller [1] argued that there were two critical strain rates, $\dot{\varepsilon}_c$ and $\dot{\varepsilon}_n$ (Section 2.1 and Fig. 4). At a given concentration, below $\dot{\varepsilon}_c$, chains remain in the coiled state, i.e. the coil–stretch transition occurs in the strain rate interval $\dot{\varepsilon}_n - \dot{\varepsilon}_c$; above $\dot{\varepsilon}_n$, chains extended as in a cooperative network. Fig. 41 schematically depicts this situation. Fig. 41(a) shows the situation when coil–stretch transition occurs and chains adopt fully extended chain conformation. Fig. 41(b) shows the structure when chains

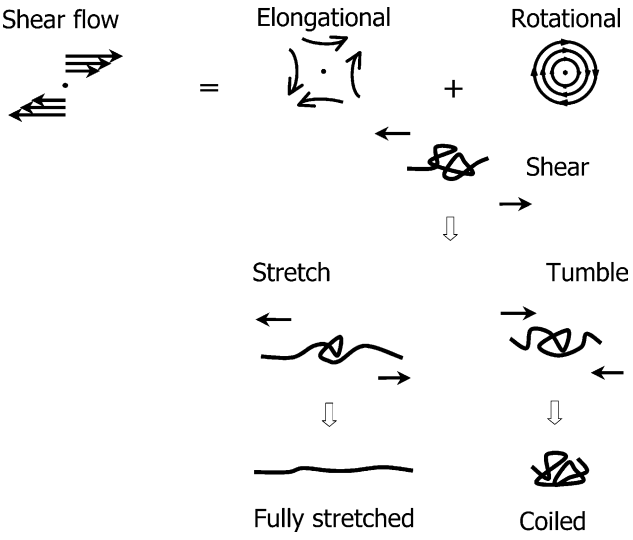

Fig. 40. A simple shear flow may be represented as a superposition of a purely rotational flow and a purely elongational flow. Schematic illustration of a flexible polymer stretching in a shear flow, as viewed in the polymer's center-of-mass frame. A velocity gradient perpendicular to the direction of flow gives rise to hydrodynamic drag forces across the molecule. These drag forces can overcome the entropic forces that tend to coil the chain and stretch the molecule along the shear axis. As the polymer stretches, many different dynamical scenarios may occur. When the chain becomes aligned, the hydrodynamic drag decreases and the chain may begin to relax. However, Brownian motion can perturb a stretched chain so that it either continues to stretch or becomes unstable and tumbles end-over-end. [Reprinted with permission from Science 1999;283:1724. Copyright (1999) The American Association for the Advancement of Science].

extend as a cooperative network. Keller observed flickering of birefringence like a flame [1] in the situation of Fig. 41(b); instead of a central bright line indicative of extended chains in Fig. 41(a). The question, whether there is a crossover, as shown in Fig. 3(b), at high concentrations or polymer melts was also addressed by Keller et al. [1]. He argued that coil–stretch transition must occur (or the

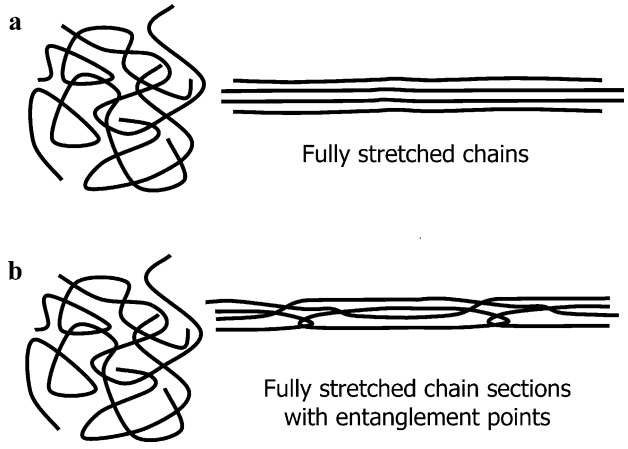

Fig. 41. Schematic diagram of the response of molecules in entangled melt under elongational flow: (a) The structure when coil–stretch transition occurs and chains adopt fully extended chain conformation, (b) the structure when chains extend as a cooperative network.

crossover is absent) in polymer melts because, (1) experiments using single jet and solid obstacles demonstrated that the elongational flow was effective at producing fibers and exhibited a lower limit on the effective strain rate; (2) there was two-fold criticality between the molecular weight and strain rate (Fig. 2), which was considered a signature of coil–stretch transition and found to be present in the formation of fibers; and (3) addition of a minute amount of ultra high molecular weight material significantly promoted fiber formation. There is no doubt about the validity of points (2) and (3) in dilute and concentrated polymer solutions, as well as in entangled melts under flow, evidenced by the recent experimental studies of chain dynamics in flow. For example, McLeash et al. [34] used a contraction device, in which the macroscopic stress field and microscopic conformation of molecules in flow was imaged optically and by small-angle neutron scattering. The scattering map revealed that the orientation at the length scale of the entire chain decayed considerably more slowly than that at the smaller entanglement length. We suspect that the cause for the above behavior is the molecular relaxation time that scales with 3.4 power of molecular weight. Thus, the finding may not establish the clear existence of coil–stretch transition. Regarding point (1), the formation of fibrous morphology is indeed the result of the crystallization of longitudinally aligned chains, but whether the individual chains were fully extended, and the coil–stretch transition occurred is still not completely evident.

It should be noted here that, according to Keller [1], the crossover must exist in the case of cross-linked systems and $\dot{\varepsilon}_n < \dot{\varepsilon}_c$ must pertain. Interestingly, the flow-induced morphological effects in cross-linked systems are similar to the morphology in un-crosslinked systems, including dilute and concentrated solutions as well as entangled melts. The morphology in cross-linked systems, Keller contended, must also arise from the fully extended chains, but now between fixed cross-links; i.e. flow coil–stretch transition occurred between fixed junctions of the network. We believe that this is an important point, which essentially formed a basis for the modified mechanism for the origin of shish, which will be discussed later.

The shish formation has always been related to the crystal growth process. As described in Section 2.2.2, Pennings et al. [101,102,129] argued that in dilute PE solutions under elongational flow, the extended chains with parallel alignment crystallize and form micellar nuclei, which extends by the flow and grows by the attachment of new chains on the lateral surface. This argument suggests that a flow field is necessary for the growth of shish crystals. In contrast, Petermann et al. [105] have carried out experiments to show that the growth of the shish crystal can occur in relaxed melt, following an autocatalytic process. This suggests that the self-orientation of the chain on the shish growth front does not necessarily require a flow field.

5.2. Modified view of shish formation—shish contain non-crystalline structures

With recent experimental evidence, it is clear that the flow-induced shish entity does not need to possess 3-dimensional crystalline orderings; it can consist of a mesomorphic or even amorphous structure. A recent review paper by de Jeu et al. [112] gives an excellent discussion of the role of mesomorphic ordering on subsequent crystallization. They listed three semi-crystalline polymers, poly(ethylene terephthalate) (PET), iPP and polydiethylsiloxane (PDES), containing typical flexible to semi-rigid chains, which all exhibit mesophase behavior under flow [112,129–135]. In these polymers, the mesophase behaves as a precursor of crystallization. The origin of mesomorphic ordering can be attributed to the induced chain rigidity by conformational ordering. They also argued that the flow-induced mesophase not only promotes nucleation and thus crystallization rate, it also forms a template that can lead to different crystal modifications, change the morphology, and guide the orientation of crystals.

The results from our in situ X-ray shear studies (e.g. Section 3.1.1—pure iPP; Section 3.1.2—iPP and aPP blends; Section 3.1.4—binary PE blends) clearly indicated that shear induces shish entities, which subsequently nucleate kebabs. However, the shish entity can consist of amorphous (e.g. oriented aPP chains in iPP/aPP blend), mesomorphic (iPP) and crystalline (PE blend) structures. The common feature in these shish is the assembly of extended chains aligned parallel to the flow direction, but they can undergo a phase transitions or simply stay stretched and oriented without changing phases. Based on SAXS and SEM measurements, we further concluded that the chains in observed shish may not be fully extended; only some portions of the chain are fully stretched and can be explained as follows.

5.3. Possible molecular mechanism for shish formation

As in the case of dilute solutions under elongational flow [30–33], the extent of orientation and/or extension of chain segments or sections of a polymer chain in an entangled melt will depend upon their initial equilibrium conformation. Note that stretching of a chain segment can occur only when the flow time scale ($1/\dot{\varepsilon}$) is smaller than segmental Rouse relaxation time; i.e. in intense flow fields [34]. The chain segments that are aligned with the flow eigenvector will orient and/or stretch. Let us consider one such chain segment that is parallel to the flow direction and referred to as '$\|$ segment' in the following. At the very early stages, infinitesimal time after imposition of flow, one polymer chain might contain many $\|$ segments, randomly located along its length. The initial, just prior to flow, orientation of chain segments will determine where the $\|$ segments are placed along the chain length. Statistically, their distribution will follow fundamental laws of

probability; some || segments will be closer to each other, while the others will be far apart.

Consider a small section of chain, of the order of persistent length, containing one || segment. Each segment in this chain section can 'sense' the orientation of the other segments. As the || segment forms, the segments in the immediate proximity, which were previously shielded, are now exposed to the full flow field. Drawing analogy from the dilute solution studies, these segments can now orient along the flow direction and the net effect is that all of the segments in the section can unwind and spontaneously undergo the abrupt coil–stretch transition, and form a fully stretched chain section. At the early stages, the fully stretched length is probably on the order of persistent length. Let us assume that 'SL' represents a stretched length associated with one '|| segment'. Due to simultaneous unwinding of many || segments, some of which are close to each other, it is likely that several segments (nSL) can combine to form a long fully stretched chain length, on the order of many persistent lengths.

The entanglement points in polymer melt keep forming and breaking up in a statistical equilibrium. The double reptation model of chain dynamics that include the concepts of CS and CCR, etc. has shown that, after deformation some of the entanglement points are completely removed. The reptation or disengagement time of the short chains is very short, and these relax or lose orientation almost immediately after cessation of flow. Many of the entanglement points associated with these chains disappear and several chain sections can become entirely free. Thus, it is possible to have considerably long fully stretched chain sections after deformation, as shown in Fig. 41(b). During deformation, multiple chain sections of the entangled mesh of several polymer chains can undergo coil–stretch transition and result in many sections with fully stretched chain lengths aligned parallel to each other. On the other hand, the chain sections that contain segments that are not aligned with the flow field and do not substantially orient, will remain entangled.

It is important to contrast the above described conceptual model for deformed melts with the situation in cross-linked systems like rubbers. In cross-linked systems, the movement/orientation of a chain segment at or near the junctions is restricted because the end of the segment is fixed; whereas in melts, the entanglement junctions are not permanent and they continuously appear/disappear with the process being very fast in flow. Consider two flow conditions: (1) Weak flow and (2) intense flow. In weak flow, chains orient but do not stretch between cross-links. At the segmental level, if one of the segments is highly oriented or aligned with the stress, the remaining chain segments of the chain section become less oriented so as to maintain the average value of the chain-section orientation. Hence, chain sections (consisting of many segments) between cross-links cannot be fully extended under weak flow. However, in polymer melt, we envision that all segments of an entangled polymer chain can cooperatively respond to the external stress. The applied stress can be distributed over the entire chain length through the entanglement points. As a result, even under weak flow condition, certain sections of a chain can be fully extended while remaining sections loose orientation or become coiled, thus maintaining the average value of the orientation corresponding to the applied stress. In intense flow (or at high strains), the chain sections can stretch, i.e. separation between junctions can increase, thus some of the chain sections between cross-links can become fully extended. This behavior would be the same as for elongational flow entangled polymer melts.

5.4. Formation of shish-kebabs with multiple shish

A single shish, containing sections of stretched chain segments separated by entanglement points (Fig. 41(b)), can nucleate kebabs in at least two possible pathways: (1) By the conventional mechanism as described in Section 2.2.1 [1], or (2) through a diffusion and subsequent adsorption process of coiled chains as demonstrated by recent simulations [28,29]. It is reasonable to assume that the stretched sections, containing extended and aligned chains with no entanglements, would be most likely to initiate the kebab nucleation; whereas the entangled sections would not. The longitudinal separation of layered kebabs along the shish, however, may be due to the nucleation events dictated by the statistics consequence rather than by the entanglement distribution along the shish.

The visual evidence of multiple shish in UHMWPE (Fig. 33) suggests the following mechanism. The dispersed UHMWPE phase in the MB-50k/UHMWPE melt should consist of multiple chains with many inter- and intra-chain entanglements because (1) the length of UHMWPE is extraordinarily long (the average contour length is over 25 μm) and (2) the UHMWPE concentration (2 wt%) is significantly larger than the overlap concentration of UHMWPE ($C^* \sim 0.2$ wt%). Thus, under deformation, not only multiple sections of chain segments in a single shish would undergo coil–stretch transition, but multiple shish having the same axial orientation can also form in a close vicinity due to the interconnectivity between the adjacent shish. The connectivity between the adjacent shish has been verified by the SEM image (Fig. 34) of the shish entities with the attached kebabs being chemically removed. It is seen that many branch points are seen between the shish, which form almost a network structure. We thus hypothesize that the presence of multiple shish may be related to the very long chain length of UHMWPE—i.e. the longer the chain length, the higher the possibility to form multiple shish, and this may be a universal phenomenon. We will verify this hypothesis with other ultra high molecular weight polymers as crystallization precursors in the future.

The observed long length of shish (on the micron scale) in Fig. 34 can be attributed to the linear connectivity of the multiple shish, since the stretched chains are more or less

pinned down and cannot disentangle. We believe that in UHMWPE, crystallization takes place in the stretch sections, forming extended-chain crystals. The entangled sections may be incorporated in the crystals as defects. We hypothesize that crystallization may not necessarily occur in some other precursor polymers, such as iPP and aPP. This is because the stable crystallographic structure in iPP (i.e. α-form) requires some specific arrangement of chain helix [107], which may not be present in the initially formed shish containing extended chain conformations. As a result, the extended iPP chain segments may transform directly into the metastable mesophase without the correct registration of helical chains as in crystallization. In the case of aPP 'shish', the chains will not be able to undergo any phase transition and may remain in the amorphous state.

Judging from the two possible pathways of nucleating the kebabs by a shish, we favor the mechanism proposed by Muthukumar et al. [28] and Frenkel et al. [29] that the kebabs are originated from the coiled chains (or coiled sections of the UHMWPE chains). It is logical to assume that shear first induced a network of shish, in which some are connected in the close vicinity because of the long chain length. One possible scenario of creating the shish-kebab morphology with multiple shish is shown in Fig. 42, which shows the absorption of a coiled chain (or a coiled segment) near the branch point of shish containing several entanglement defects. As the crystallization process occurs in the coiled chain (segment), the kebab entity may penetrate through several nearby shish. This mechanism is consistent with the SEM observations.

It should be emphasized here, as mentioned in Section 1.1, that the validity of both the concept of coil–stretch transition, introduced by de Gennes [22], and Keller's [1] model of shish-kebab structure, in existence for about three decades, in entangled melts is questioned even today by many researchers. Especially, the rheological community does not believe that chain disentanglement would occur in entangled polymer solutions and melts. Since direct observation of the polymer molten chains in flow is not yet possible, the disputes of molecular mechanisms cannot be resolved unequivocally. Nevertheless, it is our opinion that the proposed mechanism and model (Fig. 42) is a reasonable representation of the experimental results. It is hoped that the discussion in the present article will inspire new experimental measurements to pin down the exact details of the subject. Revisions and corrections of the proposed mechanism are expected.

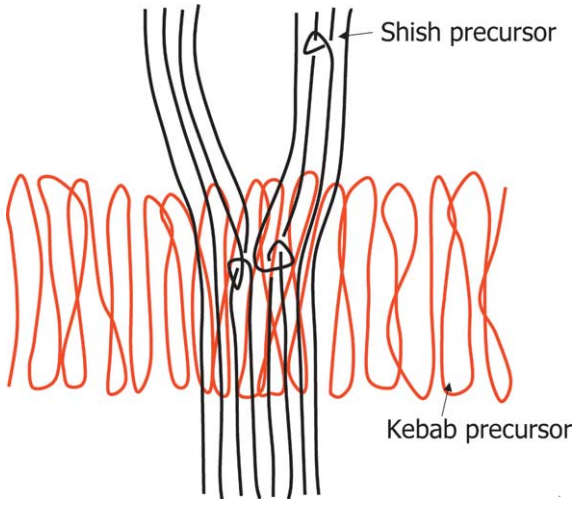

Fig. 42. Schematic diagram of the scaffold formation—the formation of kebab structure onto multiple shish. The multiple shish may be cause by the lack of ability to disentangle at the entanglement point.

6. Concluding remarks

In polymer processing, the external flow field discriminates polymer chains by their rheological behavior in the entangled melt. The resulting state of chain extension and orientation would directly influence the subsequent crystallization and morphological development, and thus the final properties. The recent studies using in situ rheo-X-ray/-optical techniques and ex situ electron microscopic methods provided ample evidence to conclude that an intense flow always creates a scaffold of crystallization precursor structures, in the form of shish-kebabs, at the initial stage of crystallization. The network-like precursor topology essentially dictates the final morphology. During precursor development, the shish formation can be best described by the concept of coil–stretch transition of de Gennes [22] and the critical orientation molecular weight (M^*) of Keller [1], while the kebab formation follows the mechanisms demonstrated by Muthukumar [28] and Frenkle [29]. Several new experimental findings including (1) that the state of shish can consist of amorphous, mesomorphic or crystalline structure, and (2) the presence of multiple shish, prompted us to modify the existing view of the shish-kebab formation. In short, in an entangled melt only sections of a chain undergo the coil–stretch transition, not the whole chain. The process results in the formation of shish-kebab structure with multiple shish containing many entanglements as well as multiple connectivities to coiled sections, which eventually form kebabs.

The above studies clearly showed the role of long chains. Without question, the long chains are primarily responsible for the formation of the crystallization precursor structure, especially shish, under flow. However, such a precursor structure can also be manipulated by the addition of long branched chains, interpenetrating networks, and nano-scale particles of different dimensionality (e.g. sphere, tube/rod, plate). The exact role of these additives on the microstructural development as well as the scaffolding formation is not clear, and remains an open subject for more in-depth investigations in the future.

Acknowledgements

The authors gratefully thank the National Science Foundation (DMR-0405432) for the support of this work. The author also acknowledges the assistance of C. Avila-Orta, C. Burger, D.F. Fang, J.K. Keum, L. Liu, A. Nogales, S.F. Ran, I. Sics, S. Toki, X.H. Zong and F. Zuo for experimental assistance. In particular, the authors wish to thank Prof F. Balta-Calleja, S.Z.D. Cheng, B. Chu, P. Geil, F. Khoury, B. Lotz, J. Schultz and S.Q. Wang for their insightful comments on several subjects.

References

[1] Keller A, Kolnaar HWH. In: Meijer HEH, editor. Processing of polymers, vol. 18. New York: VCH; 1997. p. 189.
[2] Eder G, Janeschitz-Kriegl H. In: Meijer HEH, editor. Processing of polymers, vol. 18. New York: VCH; 1997. p. 269.
[3] Wunderlich B. Macromolecular physics. vol. 2. New York: Academic Press; 1973.
[4] Keller A, Hikosaka M, Rastogi S. Phys Sci 1996;T66:243.
[5] Keller A, Hikosaka M, Rastogi S, Toda A, Barham PJ, Goldbeck-Wood G. J Mater Sci 1994;29:2579.
[6] Keller A, Cheng SZD. Polymer 1998;39:4461.
[7] Pennings J, van der Mark JMAA, Kiel AM. Kolloid ZZ Polym 1970; 237:336.
[8] Mackley MR, Keller A. Polymer 1973;14:16.
[9] Pope P, Keller A. Colloid Polym Sci 1978;256:751.
[10] Miles MJ, Keller A. Polymer 1980;21:1295.
[11] Bayer RK, Eliah AE, Seferis JC. Polym Eng Rev 1984;4:201.
[12] Ania F, Bayer RK, Tschmel A, Michler HG, Naumann I, Baltá Calleja FJ. J Mater Sci 1996;31:4199.
[13] Rueda R, Ania F, Baltá Calleja FJ. Polymer 1997;38(9):2027.
[14] Kalay G, Bevis MJ. J Polym Sci, Polym Phys 1997;35:265.
[15] Wilkinson N, Ryan AJ. Polymer processing and structure development. Dodrecht: Kluwer; 1998.
[16] Varga J. J Mater Sci 1992;27:2557.
[17] Varga J, Karger-Kocsis J. Polymer 1995;36(25):4877.
[18] Varga J, Karger-Kocsis J. J Polym Sci, Part B: Polym Phys 1996; 34(4):657.
[19] Vleeshouwers S, Meijer HEH. Rheol Acta 1996;35:391.
[20] White M, Bassett DC. Polymer 1997;38(22):5515.
[21] Goschel U, Swartjes FHM, Peters GWM, Meijer HEH. Polymer 2000;41(4):1541.
[22] de Gennes PG. J Phys Chem 1974;15:60.
[23] Doi M. J Polym Sci, Polym Lett Ed 1981;19:265.
[24] Graessley WW. Adv Polym Sci 1982;47:67.
[25] Marrucci G, Ianniruberto G. Macromolecules 2004;37(10):3934.
[26] des Cloizeaux J. Europhys Lett 1988;5:437.
[27] Mead W. J Rheol 1996;40:633.
[28] Dukovski I, Muthukumar M. J Chem Phys 2003;118:6648.
[29] Hu W, Frenkel D, Mathot VBF. Macromolecules 2002;35:7172.
[30] Perkins TT, Smith DE, Chu S. Science 1997;276:2016.
[31] Smith E, Babcock HP, Chu S. Science 1998;281:1335.
[32] Smith DE, Babcock HP, Chu S. Science 1999;283:1724.
[33] Babcock HP, Teixeira RE, Hur JS, Shaqfeh ESG, Chu S. Macromolecules 2003;36:4544.
[34] Bent J, Hutchings LR, Richards RW, Gough T, Spares R, Coates PD, et al. Science 2003;301:1691.
[35] Hobbs K, Humphris ADL, Miles MJ. Macromolecules 2001;34: 5508.
[36] Jerschow P, Janeschitz-Kriegl H. Int Polym Proc 1997;12(1):72.
[37] Haudin J, Duplay C, Monasse B, Costa JL. Macromol Symp 2002; 185:119.
[38] Bove L, Nobile MR. Macromol Symp 2002;185:135.
[39] Acierno S, Palomba B, Winter HH, Grizzuti N. Rheol Acta 2003;42: 243.
[40] Tapadia P, Wang SQ. Macromolecules 2004;37:9083.
[41] Tapadia P, Wang SQ. Phys Rev Lett 2003;91:198301.
[42] Mitchell R, Holt JJ, Thornley SA, Chai CK. Proceedings of international conference on flow induced crystallization of polymers, Salerno, Italy, 14–17 2001. p. 15.
[43] Pople JA, Mitchell GR, Sutton SJ, Vaughan AS, Chai CK. Polymer 1999;40:2769.
[44] Terrill J, Fairclough JPA, Towns-Andrews E, Komanschek BU, Young RJ, Ryan AJ. Polymer 1998;39(11):2381.
[45] Ryan J, Stanford JL, Bras W, Nye TMW. Polymer 1997;38(4):759.
[46] Ryan J, Terrill NJ, Fairclough JPA. In: Cebe P, Hsiao BS, Lohse DJ, editors. Scattering of polymers. ACS symposium series, vol. 739. Washington, DC: Oxford; 2000. p. 201.
[47] Samon JM, Schultz JM, Hsiao BS, Seifert S, Stribeck N, Gurke I, et al. Macromolecules 1999;32:8121.
[48] Somani RH, Hsiao BS, Nogales A, Srinivas S, Tsou AH, Sics I, et al. Macromolecules 2000;33:9385.
[49] Nogales A, Hsiao BS, Somani RH, Srinivas S, Tsou AH, Balta-Calleja F, et al. Polymer 2000;42:5247.
[50] Somani RH, Hsiao BS, Nogales A, Srinivas S, Tsou AH, Balta-Calleja F, et al. Macromolecules 2001;34:5902.
[51] Somani RH, Yang L, Hsiao BS. Physica A 2002;304:145.
[52] Somani RH, Yang L, Sics I, Hsiao BS, Pogodina NV, Winter HH, et al. Macromol Symp 2002;185:105.
[53] Somani RH, Yang L, Hsiao BS, Agarwal P, Fruitwala H, Tsou AH. Macromolecules 2002;35:9096.
[54] Somani RH, Yang L, Hsiao BS, Fruitwala H. J Macromol Sci, Part B: Phys 2003;B42:515.
[55] Agarwal PK, Somani RH, Weng W, Mehta A, Yang L, Ran S, et al. Macromolecules 2003;36:5226.
[56] Yang L, Somani RH, Sics I, Hsiao BS, Kolb R, Fruitwala H, et al. Macromolecules 2004;37(13):4845.
[57] Somani RH, Yang L, Hsiao BS, Sun T, Pogodina NV, Lustiger A. Macromolecules 2005;38:1244.
[58] Kumaraswamy G, Varma RK, Issaian AM, Kornfield JA, Yeh F, Hsiao BS. Polymer 2000;41(25):8931.
[59] Kumaraswamy G, Kornfield JA, Yeh F, Hsiao BS. Macromolecules 2002;35:1762.
[60] Seki M, Thurman DW, Oberhauser JP, Kornfield JA. Macromolecules 2002;35:2583.
[61] Pogodina V, Siddiquee SKS, VanEgmond JW, Winter HH. Macromolecules 1999;32:1167.
[62] Pogodina NV, Winter HH. Macromolecules 1998;31:8164.
[63] Pogodina NV, Lavrenko VP, Winter HH, Srinivas S. Polymer 2001; 42:9031.
[64] Pogodina NV, Winter HH, Srinivas S. J Polym Sci, Polym Phys 1999;37(24):3512.
[65] Duplay C, Monasse B, Haudin J, Costa J. Polym Int 1999;48:320.
[66] Devaux N, Monasse B, Haudin JM, Vermant J, Moldenaers P, Andre JM, et al. Proceedings of international conference on flow induced crystallization of polymers, Salerno, Italy, 14–17 2001. p. 31.
[67] Eder G, Janeschitz-Kriegl H, Liedauer S. Prog Polym Sci 1990;15: 629.
[68] Liedauer S, Eder G, Janeschitz-Kriegl H, Jerschow P, Geymayer W, Ingolic E. Int Polym Proc 1993;8(3):236.
[69] Kumaraswamy G, Varma RK, Kornfield JA. Rev Sci Instrum 1999; 70(4):2097.
[70] Kumaraswamy G, Issaian AM, Kornfield JA. Macromolecules 1999; 32(22):7537.
[71] Tribout G, Monasse B, Haudin J. Colloid Polym Sci 1996;274:197.
[72] Monasse B. J Mater Sci 1995;30:5002.

[73] Bassett C. Proceedings of international conference on flow induced crystallization of polymers, Salerno, Italy, 14–17 2001. p. 59.
[74] Abo el Maaty MI, Bassett DC. Polymer 2001;42:4957.
[75] Abo el Maaty MI, Bassett DC. Polymer 2001;42:4965.
[76] Li L, Jeu WH. Macromolecules 2003;36:4862.
[77] Li L, Jeu WH. Phys Rev Lett 2004;92:075506.
[78] Hsiao BS, Yang L, Somani RH, Avila-Orta CA, Zhu L. Phys Rev Lett 2005;94:117802.
[79] Strobl G. Eur Polym J 2000;E3:165.
[80] Olmsted D, Poon WCK, McLeish TCB, Terrill NJ, Ryan AJ. Phys Rev Lett 1998;81:373.
[81] Imai M, Mori K, Mizukami T, Kaji K, Kanya T. Polymer 1992;33:4451.
[82] Imai M, Kaji K, Kanya T, Sakai Y. Phys Rev 1995;B52:12696.
[83] Imai M, Mori K, Mizukami T, Kaji K, Kanya T. Polymer 1992;33:4457.
[84] Imai M, Kaji K, Kanya T. Macromolecules 1994;27:7103.
[85] de Gennes G, Pincus P. Polym Prepr 1977;18:161.
[86] Kim H, Pincus P. Biopolymers 1979;18:2315.
[87] Keller A, Machin MJ. J Macromol Sci, Phys 1967;B1(1):41.
[88] Hill MJ, Keller A. J Macromol Sci, Phys 1969;B3(13):153.
[89] Hill MJ, Keller A. J Macromol Sci, Phys 1971;B5(3):591.
[90] Keller A, Mackley MR. Pure Appl Chem 1974;39:195.
[91] Hill MJ, Barham PJ, Keller A. Colliod Polym Sci 1980;258:1023.
[92] Hill MJ, Keller A. Colloid Polym Sci 1981;259:335.
[93] Hill MJ, Barham PJ, Keller A. Colloid Polym Sci 1983;261:721.
[94] Keller A, Muller AJ, Odell JA. Prog Colloid Polym Sci 1985;75:175.
[95] Odell JA, Keller A, Muller AJ. Polymer 1985;26:1219.
[96] Rastogi S, Hikosaka M, Keller A, Kawabata HJ. Macromolecules 1991;24:6384.
[97] Odell JA, Keller A, Muller AJ. Prog Colloid Polym Sci 1992;301:270.
[98] Hikosaka M, Rastogi S, Kawabata HJ, Keller A. Macromol Sci 1992;B31:87.
[99] Keller A, Kolnaar JWH. Prog Colloid Polym Sci 1993;81:92.
[100] Mitsuhashi S. Bull Text Res Inst (J) 1963;66:1.
[101] Pennings J, Kiel AM. Kolloid ZZ Polym 1965;205:160.
[102] Pennings J, van der Mark JMAA, Booij HC. Kolloid ZZ Polym 1969;236:99.
[103] Hoffmann JD. Polymer 1979;20:1071.
[104] Petermann J, Miles M, Gleiter H. J Polym Sci, Polym Phys 1979;17:55.
[105] Lieberwirth I, Loos J, Petermann J, Keller A. J Polym Sci, Polym Phys 2000;38:1183.
[106] Chang H, Lee KG, Schultz JM. J Macromol Sci, Phys 1994;B33:105.
[107] Petermann J, Gleiter H. J Polym Sci, Polym Lett 1977;15:649.
[108] Hristov HA, Schultz JM. J Polym Sci, Polym Phys 1990;28:1647.
[109] Welsh GE, Blundell DJ, Windle A. Macromolecules 1998;31:7562.
[110] Welsh GE, Blundell DJ, Windle A. J Mater Sci 2000;35:5225.
[111] Samon M, Schultz JM, Hsiao BS. Polymer 2002;43:1873.
[112] Li L, de Jeu WH. Interphases and mesophases in polymer crystallization. In: Allegra G, editor. Advances in polymer science; Vol. 181, Chapter 2, in press.
[113] Wang ZG, Hsiao BS, Sirota EB, Agarwal P, Srinivas S. Macromolecules 2000;33(3):978.
[114] Ran S, Zong X, Fang D, Hsiao BS, Chu B, Ross R. J Appl Crystallogr 2000;33:1031.
[115] Lotz B. Eur Polym J 2000;E3:185.
[116] Alexander LE. X-ray diffraction in polymer science. New York: Wiley; 1969.
[117] Williams T, Blundell DJ, Keller A, Ward IM. J Polym Sci, Polym Phys 1968;6:1613.
[118] Keith HD, Padden FJ, Vadimsky RG. Science 1965;150:1026.
[119] Hashimoto T, Takebe T, Suehiro S. Polym J 1986;18:123.
[120] Lauger J, Gronski W. Rheol Acta 1995;34:70.
[121] Lovinger J, Chua JO, Gryte CC. J Polym Sci, Polym Phys 1977;15:641.
[122] Lovinger J. J Polym Sci, Polym Phys 1983;21:97.
[123] Meille SV, Ferro DR, Bruckner S, Lovinger A, Padden FJ. Macromolecules 1994;27:2615.
[124] Keum JK, Burger C, Hsiao BS, Somani R, Yang L, Kolb R, et al. Prog Colloid Polym Sci 2005;130:114.
[125] Hermans JJ. Recl Trav Chim Pay-Bas 1944;63:211.
[126] Stribeck N. J Phys IV 1993;3:507.
[127] Gmachowski L. Colloids Surf A Physicochem Eng Aspects 2002;201:41.
[128] Wolff T. PhD Thesis. University of Marburg; 1994.
[129] Pennings J, Pijpers MFJ. Macromolecules 1970;3:261.
[130] Hedden RC, Tachibana H, Duncan TM, Cohen C. Macromolecules 2001;34(16):5540.
[131] Koerner H, Luo Y, Li X, Cohen C, Hedden RC, Ober CK. Macromolecules 2003;36(6):1975.
[132] Ran S, Zong X, Fang D, Hsiao BS, Chu B, Phillips RA. Macromolecules 2001;34(8):2569.
[133] Ran S, Wang Z, Burger C, Chu B, Hsiao BS. Macromolecules 2002;35(27):10102.
[134] Ran S, Fang D, Zong X, Hsiao BS, Chu B, Cunniff PM. Polymer 2001;42:1601.
[135] Ran S, Zong X, Fang D, Hsiao BS, Chu B. J Mater Sci 2001;36:3071.

Rajesh H. Somani received B.Tech in Chemical Engineering from Indian Institute of Technology, Bombay, India in 1976. He completed Ph.D. in Chemical Engineering from University of Connecticut, USA in 1983, under the guidance of Professor M. T. Shaw. He spent a year at University of Massachusetts, USA working for Prof. William J. MacKnight, as a post-doctoral researcher, two years as a research engineer in polyolefins specialties division of Union Carbide, USA, and in India as an educator, senior research scientist, and manager (R&D) for about 10 years. Dr. Somani returned to the US in 1998, and joined Professor Hsiao's group in the Chemistry Department of Stony Brook University as a senior research support specialist in 1999. Over the last six years Dr. Somani has been involved in several research projects including flow-induced polymer crystallization, structure and morphology studies of advanced polymers. Dr. Somani has extensive experience in synchrotron experiments and advanced data analysis. He has authored and co-authored over 16 reviewed publications on synchrotron study of polymer processing in the past five years.

Ling Yang received her B.S. in Chemistry from Nankai University in 1996. Following obtaining M.S. degree from the Institute of Chemistry, Chinese Acadamy of Sciences in 1999, working on metallocene catalysts and isotactic polypropylene. She was admitted to Stony Brook University and joined Prof. Benjamin S. Hsiao's research group in 2000. Her PhD thesis involved the study of flow induced crystallization in various polymer systems.

Lei Zhu was born in Shanxi Province, China, in 1972. He received his B.S. degree in Materials Chemistry in 1993 and M.S. degree in Polymer Chemistry and Physics in 1996 from Fudan University. He received his Ph.D. degree in Polymer Science from The University of Akron in 2000. After two-year postdoctoral experience at the Maurice Morton Institute, University of Akron, he joined Institute of Materials Science and Department of Chemical Engineering at The University of Connecticut, as an assistant professor. His research interests include supramolecular self-assembly of discotic liquid crystals, organic–inorganic hybrid nanomaterials, and polyelectrolyte membrane fuel cells. He is recipient of NSF Career Award, 3M Non-tenured Faculty Award, and DuPont Young Professor Award.

Benjamin S. Hsiao was born in Taipei, Taiwan. He received his B.S. in Chemical Engineering from National Taiwan University in 1980 and his Ph.D. from Institute of Materials Science, University of Connecticut in 1987. He carried out his postdoctoral training at University of Massachusetts from 1987–1989 before his tenure at DuPont Fibers and then Central Research and Development for eight years. Currently, he is a Professor in the Chemistry Department and an affiliated member in the Biomedical Engineering Department in the Stony Brook University. He has been serving as the Spokesperson for Advanced Polymer PRT (X27C) Beamline at the National Synchrotron Light Source, Brookhaven National Laboratory since 1997. He became a Fellow of the American Physical Society in 2002. He is on the editorial advisory boards of Polymer; Journal of Macromolecular Science Physics; Journal of Polymer Research; High Performance Polymers; Chinese Journal of Applied Chemistry and newly established International Journal of Electrospinning and Nanofibers. His research interests are mainly in the filed of polymer physics with an emphasis on the relationships among structure, morphology, property and processing. His recent major research projects include flow-induced crystallization, nanofiber fabrication and application, and nanocomposites. He has authored and co-authored over 250 papers and book chapters as well as holds 5 patents.